



FINAL YEAR THESIS PROJECT

ROLL NO. 16BSC037

Simulation of Space Debris Trails

Author

GOTI RIDHESH

Supervisor/Mentor

MR. VAIBHAV DIXIT

*Institute : Pandit Deendayal
Petroleum University*

*Institute : Physical Research Laboratory,
Ahmedabad*

Course : B.Sc. Physics (Hons.) Department : Astronomy and Astrophysics

Co-mentor

MR. ABHISHEK GOR

*Institute : Pandit Deendayal Petroleum
University*

Department : Department of science

July 2, 2020

Contents

1	Introduction	4
2	Background	8
2.1	Coordinate system	8
2.1.1	Horizon coordinate system	10
2.1.2	Equatorial coordinate system	12
2.1.3	1st equatorial coordinate system	12
2.1.4	2nd equatorial coordinate system	13
2.1.5	Ecliptic coordinate system	14
2.1.6	Galactic coordinate system	15
2.2	Types of orbits	17
2.3	Two line element (TLE)	20
2.4	Charge coupled device (CCD)	25
3	Methods and Results	28
3.1	(1) SGP4 model and simulation	28
3.1.1	Model Results	29
3.2	(2) Simulation of the satellite trails	42
3.2.1	Noises and efficiency of CCD	42
3.2.2	Magnitude of satellite and its phase angle	51
3.2.3	Results of phase angle and magnitude	55
3.2.4	Atmospheric extinction	58
3.2.5	Point source function	63
3.2.6	Image processing	70
3.2.7	Result of satellite trails	79
3.2.8	Simulation of the trajectory of the satellite	83
4	Future scope: TLE from optical observation of the satellite	84
5	Discussion and Conclusion	85

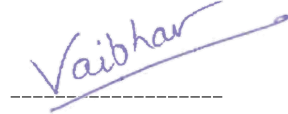
CONTENTS

APPROVAL SHEET

This dissertation titled "Simulation of Space Debris Trails" by Ridhesh Goti is recommended for the degree of Bachelor of Physics (Hons.).

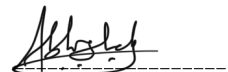
Mentor

Mr. Vaibhav Dixit



Co-mentor

Mr. Abhishek Gor



Date. 02/07/2020

CONTENTS

DECLARATION

I, Ridhesh Goti, hereby declare that this thesis represents my work in my own words and where others' ideas or words have been included, I have adequately cited and referenced the sources. I also declare that I have adhered to all principles of academic honesty, integrity, and have not misrepresented or fabricated or falsified any idea/data/fact/source in my work. I understand that any violation of the above will be cause for disciplinary action by the Pandit Deendayal Petroleum University and can also evoke penal action from the sources which have thus not been properly cited or from where proper permission has not been taken when needed.



Ridhesh Goti
Roll No. 16BSC037

Date. 02/07/2020

Simulation of Space Debris Trails

July 2, 2020

Abstract

The issues of space debris are the main space problem. The dysfunctional parts, residual parts of other satellite's collisions, and asteroids increase the density of the debris in the space continuously. The prediction of these collision needs the generalized models like SGP4 for the satellite. In the work, using the method of the SGP4 model, the precise location of the debris or satellite is obtained within the framework of the astronomical coordinate systems. Also, the TLE (Two-line element) is a set for the input to the model. The observational study of satellite trails gives the TLE. The precise result of TLE is acquired through a certain algorithm by simulating the satellite trails. The satellite trails are simulated using another method. This simulation contains many factors affecting the visibility of the trails. The factors include the noises from the CCD, atmospheric extinction, diffraction of the point source, phase angle, etc. After all, the flux of the satellite from the magnitude and quantum efficiency provides the final results of the trails. As mentioned, the simulation is useful to the algorithm to get TLE from the observational study. This work is left to future studies due to the complexity of the algorithm.

1 Introduction

The space debris could be the residual part of the satellite during the mission (anti-satellite) and collision, dysfunctional parts of the satellite, and asteroids. The space junk is a major issue considering the the increase in number of space missions. After the first launch of the satellite Sputnik in 1957, around 5000 satellites are orbiting the earth. But only 2000 satellites are

active or operational [1] and rest are dead. Also, there is around 34000 space junk with a size bigger than 10 cm. And 128 million junks bigger than 1 mm. The number is greater than the active satellites. And these junks could hit the satellites. This event could damage the satellite and produce more junks in the space [2]. The problem of space debris is very serious in the future. The trajectory of the satellite and debris should be known before the collisions. This prediction could avoid the collision by some maneuvers or techniques. ISS has done around 25 maneuvers to avoid the debris collision since 1999. But only maneuvers are not the solution to the problem. Some methods or burning of the satellites in the atmosphere are the solution to remove them completely [2]. One scientist Donald Kessler has proposed a theory 1978 that collision between satellite could cause a cascade where each collision generated the space debris which increases further collision. This effect is called collisional cascading and it happens at a high density of the debris. The effect would be more likely if the satellites are increased during the missions. The most dangerous situation is when the debris increases with exponential growth [3].

The problem is emerging in real-world problems. As mentioned earlier above, the solution to the cleaning of the junks is very complicated. Currently, avoiding the collision is the main plausible solution by knowing the exact location of two colliding satellites. The prediction of the satellite position is obtained by mathematical models. It started in 1960 by Max Lane. He developed the mathematical models for prediction using a minimal set of data elements. He introduced the analytical drag theory [4]. Furthermore, the model was modified with K. Cranford in 1969 [4]. That model included the Earth-Moon and Sun gravitational force effect with drag analysis. Lane's model was used widely for other applications like the military but after while it was improved by NORAD (North American Aerospace Defense Command) with the standard model in the early 1970s. The model takes some input parameters like inclination of the orbit, ascending node, the argument of perigee, mean motion, and eccentricity. These parameters were led to TLE (Two-line element) format which works as a punch card [31]. The furthermore development of the model with preciseness leads to publishing the model Spacetrack Report 2 [5]. The model or theory is called Air force general perturbations theory AFGP4. There are two models in the system: (1) IGP4 with drag model and (2) SGP4 (Simplified general perturbations) which also include the gravity's model [32]-[33]. Afterward, other models like SDP4, SGP8, and many more were established for geostationary satellites, low orbiting satel-

lites, etc. Using the SGP4 model, the position of the satellite in a different coordinate system is found by transformation[8]. The position of the satellite is measured in Alt-Az and Ra-Dec coordinate system. Both systems use the reference point to measure the angle in a spherical coordinate. Here, the satellite is considered which only moves around the earth, and because of that, Ra-Dec and Alt-Az coordinate systems are used in many simulations. Other coordinate systems like Galactic and Ecliptic are only useful during the planetary motions.

The prediction of the satellite orbit could help in many things like satellite trails simulation and get TLE from the optical observations. To get TLE from the optical observations, we need some constraints of the satellite and those are defined by the simulation of the actual satellite trails using some known parameters of its position and velocity. The trails of the satellite need many inputs from CCD's characteristics, atmospheric diffraction, and extinction. The CCD was invented in 1969 at Bell Labs by Willard Boyle and George Smith [11]. Because of the light-sensitive part of the CCD, it is used in many applications as a camera and TV. But the CCD has certain noises that create the blurriness of the image. In the model, the specifications of CCD are useful for creating a realistic picture of the trails with including these noises. CCD also takes the images of the stars or planets. It contains pixels with a range of micron in size and works based on the p-n junction in semiconductor[9]. In astronomy, the image output is in grayscale because mostly single-channel images are taken in astronomy. This output represents a better contrast to discern stars and other objects. The output could be in another single-channel mode like red or blue. But here, the images are in grayscale. Also, there are noises associated with these instruments like sky background, readout, shot, dark noise for the image [10]. These noises are related to thermally, source, and during the readout of the image. The noise follows Poisson or Normal distribution. Some of the noises are redundant but others are very random. The noise makes the image very blur. The blurriness is removed by reducing the noise using a standard model of them [10].

Alongside with noise, the diffraction is another factor that affects the resolution of the point source images like satellites. The diffraction occurs for any aperture but the strength for these various apertures would be different. Mostly, the diffraction dominates as the aperture size tends to the

wavelength. The diffraction term was coined by Maria Grimaldi and the experiment was performed by Thomas Young in 1665 [12]. He observed the spreading of a point source from the single slit diffraction. The diffraction affects the point source image and it results in the Gaussian point spread function [13] and makes it blur. The diffraction effects could be related to telescope aperture or the atmospheric seeing effect. And the atmospheric seeing effect is appeared due to turbulence. The diffraction occurs mainly due to the atmospheric seeing effect or aperture of the telescope. But the cumulative effect of both events results in the final image. The dominant effect of one of these depends on the wavelength, the diameter of the telescope, and the fried parameter [16] which define the strength of the diffraction [14] and [15]. This gives certain conditions [17] with the dependency of these parameters. The conditions and strength of the diffraction have certain calculations using fwhm (full width half maximum) [13]-[17]. The fwhm defines the spread of the image due to the diffraction. With diffraction, another effect called Aliasing is very essential during the image processing of the image. The aliasing effect makes the image less resolved with sudden sharp contrast. The rate of image processing or sampling rate is a vital factor to reduce it. The effect is reduced or avoided by setting a particular frequency or limit which is called the Nyquist sampling rate [18]. The theorem of the Nyquist is useful in many electronics for the processing of the data. The aliasing effect [19] is also reduced by point spread function for the point image.

The associated problems of noises, diffraction, and aliasing effect are resolved if certain constraints are applied to the model. But the image is formed by the illumination of the pixels and the illumination is done by photons coming from the source. This is called flux of the photons [20]. The flux, magnitude, brightness of an object are associated with certain functions. The magnitude of the stars is standard using observational study but for the satellites, the magnitude [21] is defined by particular function with the relation of satellite's albedo, distance to the observer, and phase angle. The phase angle is the angle between satellite to sun direction and satellite to earth. A particular angle, the satellite is illuminated with great intensity like Moon's phases [48]. Also, the magnitude of the object is decreased with distance in the earth's atmosphere. This is called atmospheric extinction [23]. The extinction occurs due to scattering or absorption of the molecules during the trajectory of the photons from the object. The attenuation of the magnitude due to the extinction leads to the reduction of the flux or brightness of the object. The

extinction happens at three stages ozone, aerosol, and other gases [24]-[25].

With all these parameters, the magnitude of the satellite is very easy to get without observation of it. But the relation needs certain reference star's magnitude like Vega. And the output of the magnitude is in visible range and flux of the object would be only within the bandwidth of the visible range. These flux of photons illuminate the pixel and create the voltage. The digital output of the CCD is obtained by considering quantum efficiency, exposure time, and the area of the telescope aperture. The quantum efficiency is the efficiency of CCD to convert the flux of photons to electrons. And the exposure time is the amount of time for the image to capture within a certain field of view. The imaging of the point satellite is done in a particular frame of the field which is called the field of view [26]. Before going to the simulation of the satellite trails, the basic coordinate systems are used to understand the output of the models. The next section describes the necessary details about the coordinate system used in astronomy.

2 Background

The coordinate systems are very essential in astronomy to understand the location of the satellite or star in the certain frame. The coordinate system and the types of orbits of the satellite are defined in further sections.

2.1 Coordinate system

As mentioned earlier, the collision between debris and satellite is main issue in the space. The simulation of space debris is required to avoid or predict such types of collisions. Before going towards simulation, the coordinate system for the earth's satellite objects needs to be explained. In astronomy, the coordinate system is different from the Cartesian coordinate system. All the coordinate systems in astronomy and daily used systems have lied to euclidean space. But the different coordinate system is used for different situations. **Astronomical coordinate systems** have different reference axis and points for measurement to avoid the inertial movement of the earth's rotation and rotation axis. There are a total of four types of the coordinate system in astronomy [27],

(1) Horizon

- (2) Equatorial
- (3) Ecliptic
- (4) Galactic

Before going into details of these coordinate systems, the basic thing for these all coordinate systems is the celestial sphere. The **celestial sphere** is a sphere with the center of observer and stars or satellites lie on the sphere. The **great circle** is a circle passing through a sphere with the greatest radius at any point. The **hour circle** is a great circle passing through poles of the celestial sphere [28].

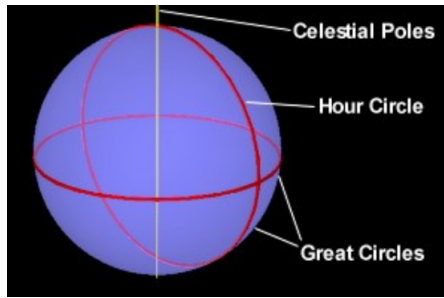


Figure 1: Celestial sphere, hour circle, and great circle

Also, position of observer is defined by **latitude** and **longitude** on the earth. The fundamental plane is **equator** of earth from where latitude is measured. The **zero point** or reference point from where longitude is measured. Zero-point passes through Greenwich, England. Longitude lines are called as **meridian** and the one passes through zero points is called as **prime meridian** [28].

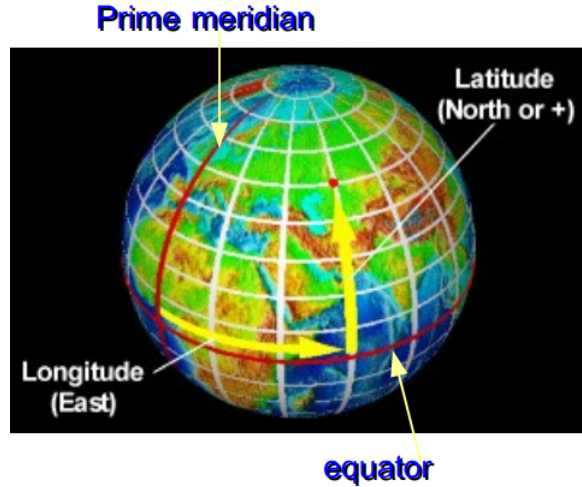


Figure 2: Latitude and Longitude

In figure 2, the latitude is a point's angular distance above or below the equator. It ranges from 90 north (positive) to 90 south (negative). Longitude is a point's angular position east or west of the prime meridian in units ranging from 0 at the prime meridian to 180 east (+) or west (-) [28]. These basic terminologies would be helpful to imagine these different types of coordinate systems. The below subsections describe the various coordinate systems, especially in astronomy. The description of these coordinate system gives only the necessary information like its basic parameters to locate the position of the satellite. For example, in horizon system, only altitude and azimuth are used to locate position of the satellite with respect to the observer.

2.1.1 Horizon coordinate system

Basic terminologies of this coordinate system are **zenith**, **nadir**, **celestial meridian, and horizon**. The point above the observer on the celestial sphere is zenith point and below the observer is nadir point opposite to zenith on celestial sphere as shown in figure 3. Zenith and nadir point are at 90 from horizon with respect to observer. The **celestial meridian** is great circle which intersects the zenith, the nadir, and the celestial poles. And perpendicular to zenith-nadir axis is called as **astronomical horizon plane** [28].

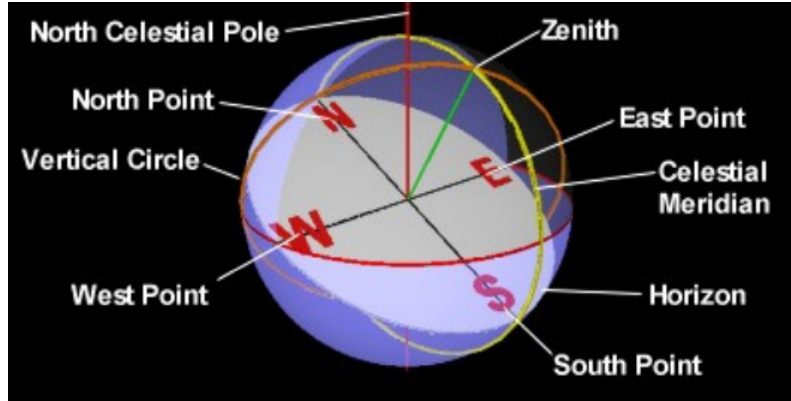


Figure 3: Horizon coordinate system

In the figure 3, **north point** is intersection of the celestial meridian and the horizon that is also closest to the north celestial pole. The **south point** is the other intersection point. **East and west points** lie at the intersections of the horizon and the celestial equator. The equator is perpendicular to the celestial meridian for example, earth's equator. Clockwise, the east point is 90 from the north point [28].

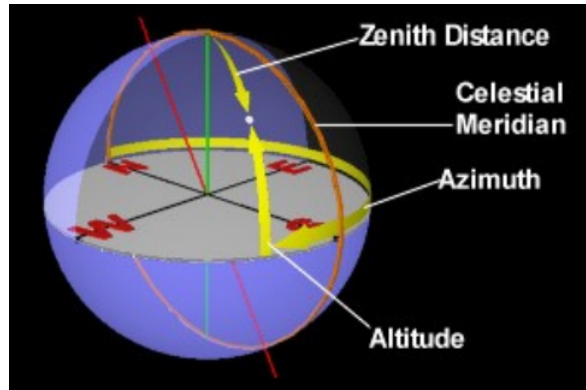


Figure 4: Altitude and Azimuth in horizon coordinate system

After deciding the points on the celestial sphere, in figure 4, the **Altitude (a)** is the angular distance between horizon and star or satellite along the vertical circle passes through satellite or star. The range of altitude is from 0 to 90 degrees. **Azimuth (A)** of a body is its angular distance measured eastwards along the horizon from the north point to the intersection of the

object's vertical circle (0 to 360 degree). **Zenith distance** is compliment of altitude $90 - a$ [28]. Suppose, the location of an object is $(a, A) = (30, 50)$ in degrees. That means, the object is 30 degrees upwards to the observer and 50 degrees eastward from the north point. Many telescopes use the altitude-azimuth horizon coordinate because of low cost and high stability. The main disadvantage of this coordinate system is that it varies with location on the earth. Therefore, we need a universal coordinate system that is constant for every observer on the earth. The equatorial coordinate system is one option that could give the same results regardless of the observer's location on the earth.

2.1.2 Equatorial coordinate system

The equatorial coordinate system has two parts, first is **1st equatorial coordinate system (hour angle)** and second is **2nd equatorial coordinate system (right ascension)**. Both coordinate systems give the same result regardless of observer location but the reference axis and point of them are different.

2.1.3 1st equatorial coordinate system

A celestial equator is a plane passing through the equator of earth and **declination** is angle δ measured along the great circle passes through satellite from the equatorial plane. At the equator, the declination is zero and it is positive, negative above and below the equator, respectively. The range of declination is from +90 to -90. Another parameter to define satellite along the equator is **hour angle (HA)** which is measured between the meridian of satellite and celestial meridian in the west direction of the celestial sphere.

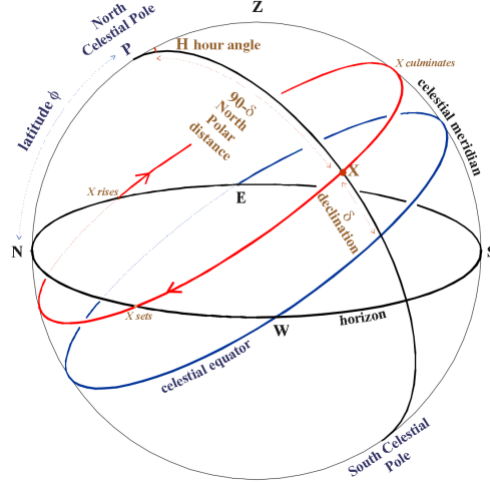


Figure 5: 1st equatorial coordinate system

The **transformation** between the horizon coordinate system to the 1st equatorial coordinate system is matrices multiplication of its component by rotation matrix for each direction x, y , and z . The transformation equation for 1st equatorial to horizon system is given by the below equation,

$$I(a, z) = R_3(180) \cdot R_2(90 - \phi) \cdot I(h, \delta) \quad (1)$$

In the equation 1, the a, z, h , and δ are azimuth, zenith distance, hour angle, and declination. Here two rotation matrices are applied to equatorial components. ϕ is the latitude of the observer [28]. After the 1st equilateral system the second one is given in next section.

2.1.4 2nd equatorial coordinate system

The ecliptic plane is the trajectory plane of the earth around the sun in space. The angle between the equator and **ecliptic plane** is 23 degrees 26 minutes. The intersection of the ecliptic and celestial equator defines the **vernal equinox** and autumnal equinox. Hour circle is a great circle that passes through celestial poles and is perpendicular to the celestial equator. The fundamental reference circle is the celestial equator and zero points are vernal equinox as shown in figure 6. The vernal equinox direction is constant for all observers on the earth. The **right ascension** (RA) of a point is the

angular distance measured eastward along the celestial equator between the vernal equinox and the hour circle intersecting the point. It is measured in hours, minutes, and seconds from 0 to 24 hours. Another parameter is declination which is the same as in 1st equatorial system.

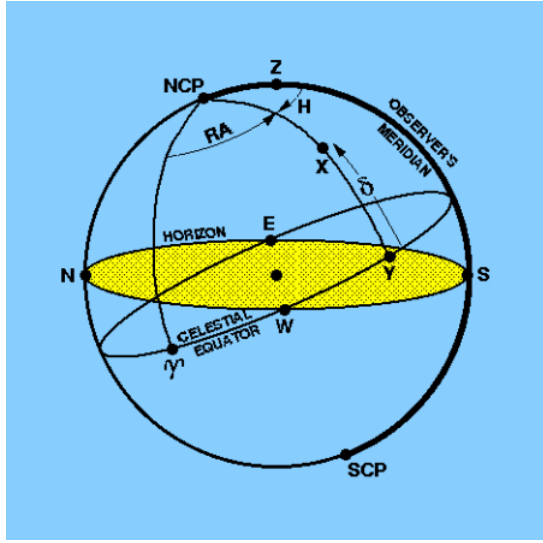


Figure 6: 2nd equatorial coordinate system

The direction of RA is defined in figure 6. To convert from 2nd equatorial to horizon system, **local sidereal time** need to be understood. Our clocks are set to run (approximately) on solar time (sun time). But for astronomical observations, we need to use sidereal time (star time). The Earth rotates 365 times relative to the Sun, but 366 times relative to the stars. So the sidereal day is about 4 minutes shorter than the solar day. Local sidereal time (LST) is an hour angle of the vernal equinox. Finally, $HA = LST - RA$ is an equation to convert RA to HA. Using equation 1, transformation between HA to azimuth angle is possible [28].

2.1.5 Ecliptic coordinate system

When dealing with the positions and motions of solar system's objects, it is often more convenient to refer positions to the mean orbital plane of the solar system using ecliptic coordinates. Fundamental circle is the ecliptic and zero point is vernal equinox. **Ecliptic latitude**, β , is analogous to declination,

but measures distance north or south of the ecliptic, attaining +90 at the north ecliptic pole (NEP) and -90 at the south ecliptic pole (SEP).

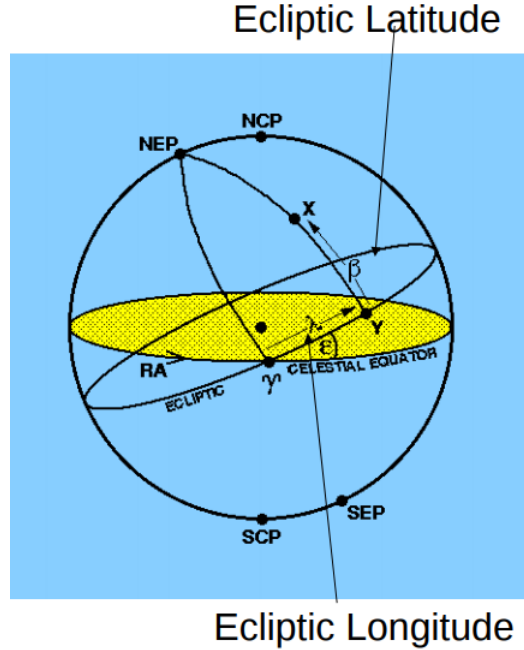


Figure 7: Ecliptic coordinate system

In the figure 7, the **ecliptic longitude**, λ , is analogous to right ascension and is measured from the vernal equinox, in the same direction as right ascension but along the ecliptic rather than the celestial equator. The transformation between 2nd equatorial system to ecliptic is given by,

$$I(\lambda, \beta) = R_1(\epsilon) \cdot I(\alpha, \delta) \quad (2)$$

In the equation 2, λ , β , α , and δ are longitude, latitude, right ascension, and declination, respectively. ϵ is obliquity of ecliptic plane with equator[28]. The transformation matrices are useful to get horizon to equatorial or ecliptic to horizon system.

2.1.6 Galactic coordinate system

The fundamental circle is galactic equator (the great circle) on the celestial sphere that represents the path of the Milky Way Galaxy. The plane is

inclined at an angle of 62.87 degrees to celestial equator.

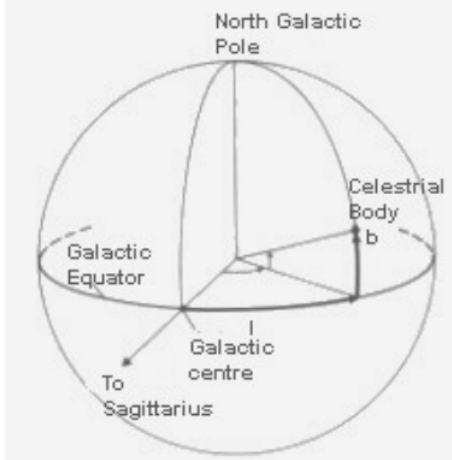


Figure 8: Galactic coordinate system

Zero-point lies in the direction of the galactic center as seen from Earth. **Galactic latitude** (b) of a celestial body is its angular distance north (+) or south (-) of the galactic equator (it ranges from 0 to 90). **Galactic longitude** (l) of a celestial body is its angular distance (from 0 to 360) from the nominal galactic center measured eastwards along the galactic equator to the intersection of the great circle passing through the body [28].

These are all types of the celestial coordinate system. Precession, nutation, proper motion, parallax, refraction are factors cause the deviation of star position. Earth's axial precession is like a spinning top, the direction of the rotation axis executes a slow precession with a period of 26,000 years. **Precession** of vernal equinox occurs due to the changing orientation of the equatorial plane. As a result, the intersections between the celestial equator and the ecliptic (the equinoxes) move along the ecliptic at a rate of about 50.27 arc seconds per year. To avoid the precession of the vernal equinox, we use standard years (like 1950, 2000, 2050) to cite the Equinox. Currently, we use the Equinox J2000.0. **Nutation** is a small cyclical motion superimposed upon the 26,000- year precession of the Earth's axis of rotation. It is mainly caused by the gravitational attraction of the Sun and Moon, which continuously change location relative to each other and thus cause nutation in Earth's axis. **Proper Motion** is the apparent motion of a star across the celestial sphere at right angles to the observer's line of sight; any radial

motion (toward or away from the Sun) is not included. It is observed with respect to a framework of very distant background stars or galaxies. **Parallax** is the angular displacement in the apparent position of a celestial body when observed from two widely separated points. **Atmospheric refraction** causes astronomical objects to appear higher in the sky than they are in reality. This effect even lifts objects from up to 35 arc minutes below the horizon to above the apparent horizon. After getting knowledge of the coordinate systems, it is very easy to get the position of the satellite in any of these systems. To get the position of the satellite with better prediction, we need to understand the orbital parameters like inclination, ascending nodes, and many more. These parameters are delivered in a very compact form of two lines. It is called the two-line element (TLE). Before going to understanding the TLE, the types of the orbits should be known to us.

2.2 Types of orbits

The types of orbits of the satellite are defined based on the altitude of them. There are three types of Earth orbits: high, medium, and low earth orbit. The most scientific satellites like remote sensing, Hubble space telescope, ISS orbit at low earth orbit. The navigation system and other special monitors of a region are analyzed by medium earth orbits.



Figure 9: The low earth orbit and medium earth orbit

In figure 9, the blue dark region describes the low and medium earth

orbits. And the velocity of the satellite is determined by its distance from the earth [29] and [30]. The high earth orbits are geosynchronous or geo-stationary orbit because they complete the orbit with the same time-period of earth's rotation. These satellites are used for telecommunications. Other than geostationary, polar orbits are another type of the satellite which passes through the poles of the earth. Within 30 degrees of the earth's poles, these satellites track the weather and prediction.

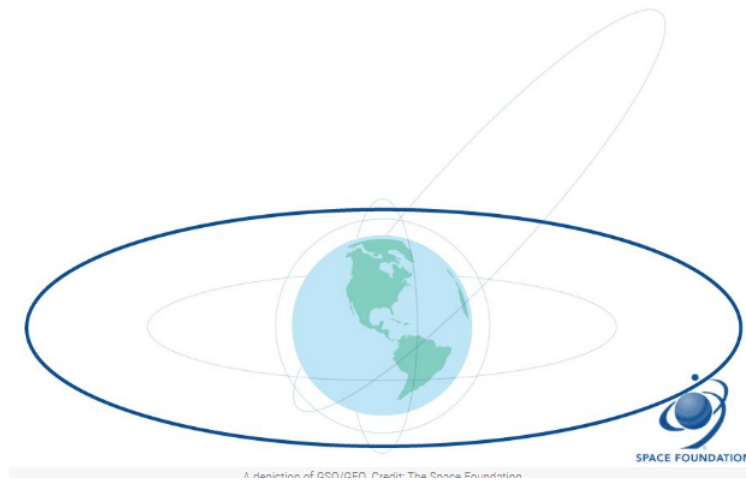


Figure 10: The high earth orbit

Sun-Synchronous Orbit is a type of polar orbit. They are synchronous with the sun and passed through the same region at the same local time every day. Another type of orbit is highly elliptical orbit.

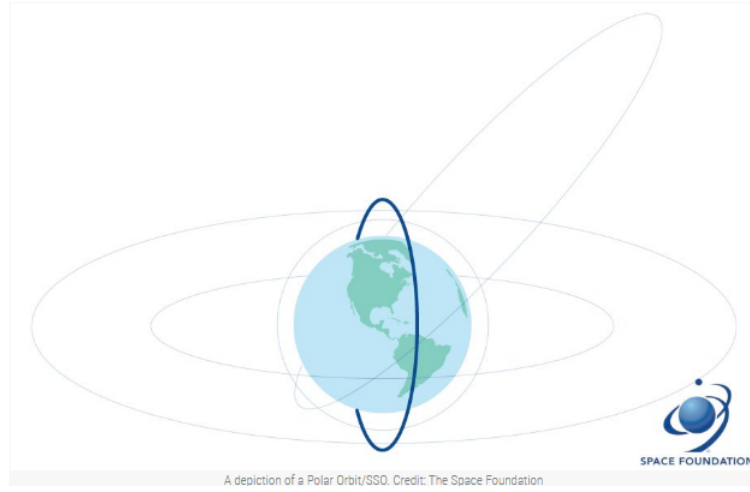


Figure 11: The polar orbit

One end of the highly elliptical orbit (heo) is near the earth and other at a very far distance. The application of this satellite is remote sensing and radio telecommunications. The range of the main three types of satellites are as follows: The low orbit has 180 to 2000 km. The medium orbit has 2000 to 35780 km. This type contains the highly elliptical orbit. The high orbit has altitude greater than 35780 km.

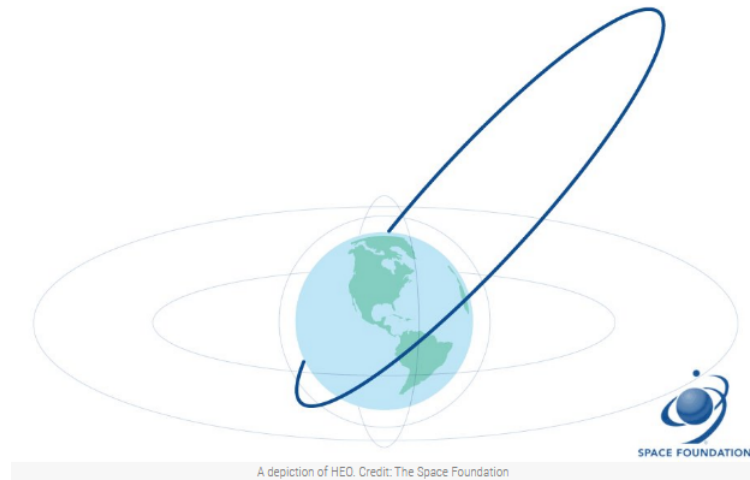


Figure 12: The highly elliptical earth orbit

The orbiting satellites in any type of the orbit have certain perturbations from the moon's, earth's gravity, drag motion, and other effects. These effects and orbits are described by the certain standard parameters like ascending node, mean motion, first-time derivative, inclination, eccentricity, etc. The compact form like punch cards is represented by the TLE. The TLE of the satellite includes its future by considering all the effects. The TLE form's components are explained in the next section.

2.3 Two line element (TLE)

A two-line element (TLE) set, an example of which is written below, is a data format describing the keplerian elements of Earth-orbiting satellites:

```
1 27843U 03031D 14297.79709235 .00000190 00000-0 10887-3 0 703
2 27843 98.7177 303.6579 0008799 278.1894 134.1004 14.20414232586768
```

A TLE set [31], together with the Standard General Perturbations satellite orbit model 4 (SGP4) model [32]-[33], can be used to determine the position of a satellite at any particular time. Here TLE works as the input for the SGP4 to predict the position of the satellite. TLE elements are used in the propagation of the orbit using epoch, inclination, right ascension of the ascending node (RAAN), eccentricity, argument of perigee, mean anomaly, mean motion and drag term. The other elements either identify the satellite (satellite number and international designator), check the data integrity (checksum), or provide additional information.

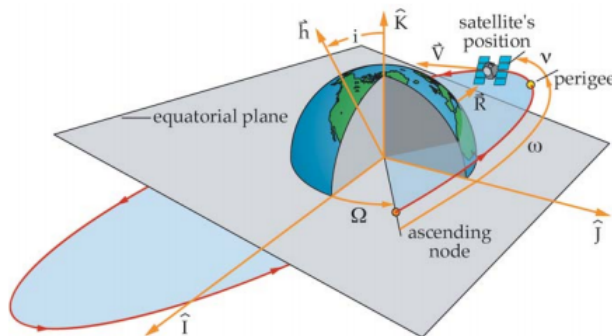


Figure 13: Inclination, ascending node, eccentricity

In the figure 13 describes the inclination angle (angle between satellite orbit and equatorial plane), ascending node (angle between intersection point and vernal equinox direction), and eccentricity (the anomaly of the orbit from the circular orbit). Another magnitude is perigee which is the closest distance between satellite's orbit to earth. And the angle between perigee point described in the figure 13 and intersection point or ascending node. These terms are described very well in the figure. The TLE doesn't contain only inclination, eccentricity, right ascension but other terms like mean motion, time derivative, and drag factor which are useful in the perturbation of the satellite's location. The description is given below in the figure with explanation.

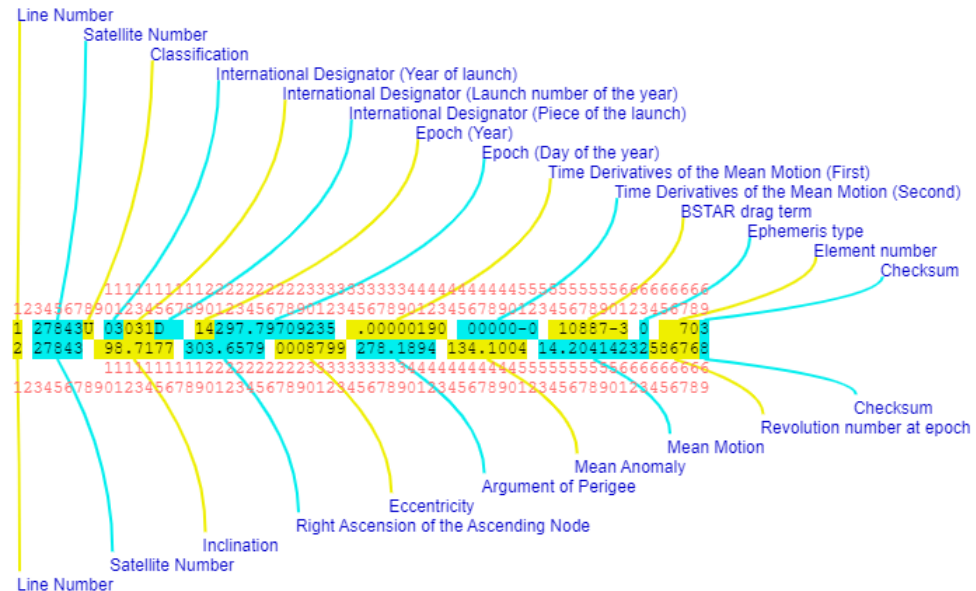


Figure 14: Two line element

In the figure 14, the first line in the TLE can be thought of as giving properties of the satellite itself, including its identifier, launch properties, and drag terms - which are determined by the cross-section and mass of the satellite [34]. The description of each term is given below,

Line Number: The line number, as the name suggests, gives the line number within the TLE. (Figure 14)

Satellite Number: The satellite number is referred to as the NORAD Catalog Number, NASA catalog number, USSPACECOM object number, or simply Catalog number. The satellite number is a unique sequential 5-digit number assigned by United States Space Command (USSPACECOM) for each earth-orbiting artificial satellite in their Satellite Catalog (SATCAT). The satellite number is assigned based upon when the object was first observed. For a TLE to be valid the satellite number in line 1 must be identical to the satellite number in line 2.

Classification: The classification indicates the security classification of the data: all publicly available data will have a 'U' in this field to indicate unclassified data.

Year of launch: Year of launch gives the last two digits of the year of launch. As no artificial satellites existed before 1957 (Sputnik 1 was launched into orbit on October 4th, 1957) values in the range from '00' to '56' are assumed to correspond to years in the range 2000 and 2056. Values in the range from '57' to '99' are assumed to correspond to years in the range 1957 to 1999.

Launch number of the year: Launch number of the year gives the launch number, starting at 1, of the given year.

Piece of the launch: The pieces of the launch are denoted by alphabetic characters, excluding the letters 'I' and 'O'. The 1st piece of a launch is denoted by 'A', and subsequent pieces 'B', 'C', 'D'... 'Z'. The 25th piece would be denoted by 'AA', and subsequent pieces 'AB', 'AC'... 'AZ', 'BA', 'BB', 'BC',... 'ZZ'.

Epoch year: Epoch year gives the last two digits of the year of the epoch.

Epoch day of the year : Epoch day of the year is the day of the year. A value of 1.0 corresponds to the midnight between December 31st and January 1st. The fractional part of the epoch day gives the time within the day, to an accuracy of approximately 1 millisecond.

First Time Derivative of the Mean Motion: This field gives the first time derivative of the mean motion divided by 2. The two time derivatives of the mean motion values give a second-order picture of how the mean motion

is changing with time, although it should be noted that these values are not used by the SGP4 orbital model.

Second Time Derivative of the Mean Motion: This field gives the second time derivative of the mean motion divided by 6. A leading decimal point is assumed and the last two characters give the applicable power of 10. For example : 12345-6 is read as $0.12345 \cdot 10^{-6}$.

BSTAR drag term: The BSTAR drag term is also referred to as the B^* drag term or the radiation pressure coefficient. Here, B^* is defined by $B = \frac{B \cdot \rho_0}{2}$. B is a ballistic coefficient and ρ_0 is atmospheric density and B is defined by $B = \frac{C_D \cdot A}{M}$. C_D, A, M are drag coefficient, the cross-section area of satellite, and mass of the satellite.

Ephemeris type : The ephemeris type (i.e. orbital model) used to generate the data. 1=SGP, 2=SGP4, 3=SDP4, 4=SGP8, 5=SDP8. These are all the present models for different applications. The default value of TLE is 0 which is equivalent to consider the SGP4 model.

Element Number: The element set number is a running count of all TLE sets generated by USSPACECOM for this object.

Checksum: The checksum is used to help prevent transcription errors in the TLE set. To calculate the checksum, simply add the values of all the numbers on each line (ignoring all letters, spaces, periods, and plus signs) and assigning a value of 1 to all minus signs.

Line 2: The second line in the TLE can be thought of as giving the properties of the orbit of the satellite.

Line number: The line number, as the name suggests, gives the line number within the TLE.

Satellite number: The satellite number is also referred to as the NORAD Catalog Number.

Inclination i_0 : The angle, in degrees, between the equatorial and the orbital plane. The value lies between 0 and 180.

Right Ascension of the Ascending Node Ω_0 : The angle between the vernal equinox and the point where the orbit crosses the equatorial plane (traveling north). The value lies between 0 and 360.

Eccentricity e : The eccentricity of the orbit. A leading decimal point is assumed, such that if the value appears as 0008799 is understood to mean 0.0008799.

Argument of perigee ω_0 : The angle between the ascending node and the orbit's point of closest approach to the earth (perigee). The value lies between 0 and 360.

Mean anomaly M_0 : The angle, measured from perigee, of the satellite location in the orbit referenced to a circular orbit with a radius equal to the semi-major axis. The value lies between 0 and 360.

Mean motion n_0 : The value is the mean number of orbits per day the object completes.

Revolution number at epoch: The period from launch to the first ascending node is considered to be revolution 0 and revolution 1 begins when the first ascending node is reached.

Checksum: It is the same as line 1's checksum.

The format of TLE is given by,

```
1 NNNNNC NNNNNAAA NNNNN.NNNNNNNN +.NNNNNNNN  
+NNNN-N +NNNN-N N NNNNN  
2 NNNNN NNN.NNNN NNN.NNNN NNNNNNNN NNN.NNNN  
NNN.NNNN NN.NNNNNNNNNNNNNNN
```

N is any digit 0-9 or, in some cases, a space. A is any character A-Z or a space. C is a character representing the classification of the element set, which is always U for publicly released data. + is a space, a minus sign, or

a plus sign (which is equivalent to a space). All the description of the TLE is taken from [34]. After getting information of satellite's parameters which define the trajectory, the model SGP4 is used for position determination. The method to find the location of the satellite is given in further section using SGP4 model. There is another information which is necessary to explain. In the second method, I simulated the satellite trails. And the satellite trails are sensed or obtained by the instrument called CCD. The details of the CCD and its associated specifications are required to get realistic trails. The next describes the general information of the CCD.

2.4 Charge coupled device (CCD)

Charge-Coupled Devices (CCDs) were invented in 1970 and originally found applications as memory devices. Their light-sensitive properties were quickly exploited for imaging applications and they produced a major revolution in Astronomy. CCD is a highly sensitive device for detecting photons from celestial objects. It is made up of a large number of light-sensitive small areas which are called pixels. The photon ejects the electron from one pixel, and electron works as data of that particular photon. The basic principle behind CCD is the photoelectric effect. The electron will be released when photon energy exceeds the work function of the material. Based on the number of electrons in each pixel, the intensity profile will be obtained [39]. The liberation energy of electron from material is given by $E = h \cdot \nu$.

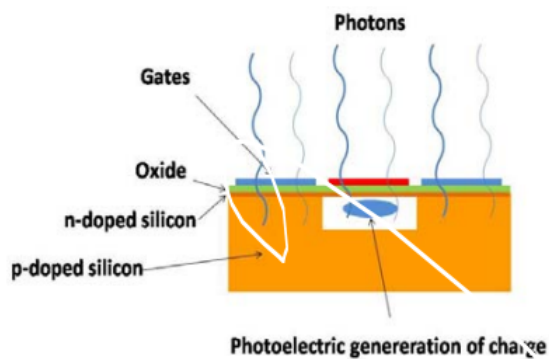


Figure 15: Generation of electron

Figure 15 describes the generation of electrons from a pixel. Photons incident on a plate and generate the electrons. Pixel is made up of metal oxide, p-type and n-type semiconductor materials. Two gates are used for transportation of charges from one pixel to another for data analysis [22] as shown in the below figure.

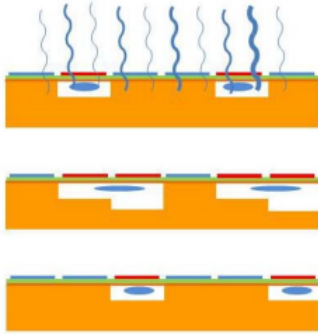


Figure 16: Transfer of charge in CCD

A potential well is a place where electrons will be stored using positive bias at the metal electrode. As more and more light falls onto the CCD, then the potential well surrounding this electrode will attract more and more electrons until the potential well is full (the amount of electrons that can be stored under a pixel is known as the full well capacity). To avoid full capacity, CCD needs a shutter to prevent photons. That's why the exposure time is a necessary thing for the imaging. CCD has rows and columns on its top plate and size is defined by a number of rows and columns. The resolution of the CCD is defined by the size of the pixels, also by their separation. In most astronomical CCDs the pixels are touching each other and the CCD resolution will be defined by the pixel size, typically $10\text{-}20 \mu\text{m}$ [22].

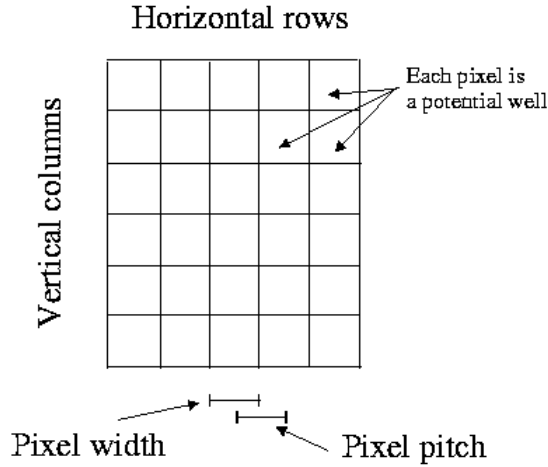


Figure 17: Pixels arrangement in CCD

In figure 18, the charges are transferred vertically downwards, then horizontally transportation is done using gate voltage. This type of process is described in the below figure. The data of each pixel is transferred vertically with the bias gate to the end of the CCD or row in a particular column. Then the results of the particular row are processed. Eventually, the image is generated after this systematic process.

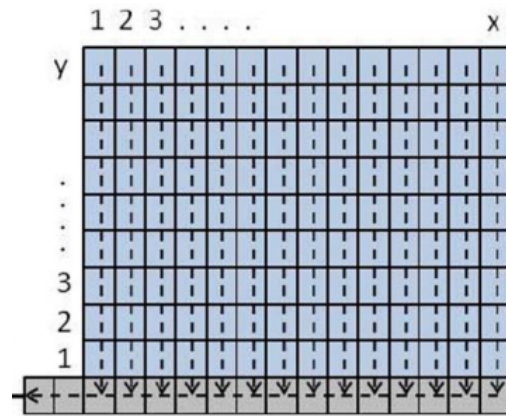


Figure 18: Pixel readout process

The output of each pixel is in an analog mode and that needs to be

converted into digital form. After processing the data, the intensity profile is created. The output is in grayscale with using certain filters. A combination of filters gives the final colored image of celestial objects. There are other factors like the efficiency of charge transfer and noise. All these contribute to the low resolution of the image. There are some mathematical techniques to reduce this kind of inaccurate data involvement [22]. But before discussing the noises and its results, the result of the SGP4 model is given in the next section. The results include the prediction of three satellites using their respective TLEs.

3 Methods and Results

The model is formulated using certain methods. The methods are divided into two parts: (1) The prediction of the position of the satellite using the SGP4 model and (2) Simulation of the trails considering all affecting factors to image processing like noise, quantum efficiency, point spread function, and atmospheric extinction. The first is focused on the SGP4 model to get the precise location of the satellite or debris. To simulate the trails of the satellite, we need the first method to find the future trajectory of it. After the SGP4 model, the trails simulation needs the realistic picture of the satellite's point image using CCD's noises, sky noise, diffraction, atmospheric extinction, and phase angle. The first method is described with the results in the below section.

3.1 (1) SGP4 model and simulation

The SGP4 stands for a simplified perturbations model [33]. During the flight of satellite or space debris, its trajectory continuously changes its parameters inclination, right ascension, time period, etc because of external perturbations from the sun, moon, earth's precession, and nutation. The model contains very complicated factors. The python has a package called SGP4 which considers all these factors for low orbiting satellites like space debris [35]. The model takes the input of TLE and time in UTC. It will give a response in the XYZ coordinate in the ECI frame. ECI (Earth-centered inertial frame) considers the center of the earth as the origin. The x-axis is the line passing through the vernal equinox. The y-axis is perpendicular to x in the direction of z cross x. The z-axis is the rotation axis of the earth. Using

the ECI frame, right ascension and declination could be found very easily. Right ascension is the angle between satellite and vernal equinox or x-axis [33]. The declination is the angle between the vector of satellite and plane XY.

The python editor is used to find RA (right ascension) and Dec (Declination). And all manipulation of the transformation is done between RA, Dec to altitude (Alt), and azimuth (Az) angle. The transformation needs latitude and longitude of the location. Because the Alt-Az system depends on the location of the observer while RA-Dec is independent of the observer's location. The transformation also includes the Julian day from the year 2000. The results of the satellite's position are given below. It is very hard to describe the whole model here because of many complex parameters related to perturbations. But the necessary results are shown in the below section.

3.1.1 Model Results

In this subsection, the results of the satellite's coordinates are obtained through the simulation of the SGP4 model using Python. The SGP4 model as mentioned is very complicated and includes so many perturbations like solar radiation, moon and earth's gravity, etc. The main input of the SGP4 model is the TLE of the satellite. The implementation of the SGP4 model in Python is done by Brandon Rhodes [35]. As the input of the model is TLE lines, the output is given in ECI coordinates and in terms of position and velocity components at given particular time. The frame of reference that is used in output is ECI (Earth-centered inertial). ECI has an origin at Earth's center. Its x-axis is the same as the direction of vernal equinox direction. In the model, (1,0,0) is taken as vernal equinox direction with origin as Earth's center. The z-axis of the frame is the rotation axis of Earth and (0,0,1) in the model, and the y-axis is a cross product of z and x [36]. After deciding all the axes, the coordinates of position and velocity in the ECI frame, which are called Phase points, are converted into Right ascension and Declination. The Ra and Dec are obtained through simple geometry and calculating the angles between vernal equinox direction and projected satellite vector direction on the XY plane. Dec is calculated by measuring the angle between the satellite vector and the projected satellite vector on the XY plane. The projected satellite vector on the XY plane is the equator of the earth. The code is given in the footnote's link. RA and Dec are independent of the observer

3 METHODS AND RESULTS

position and the results are given below;

The TLE data of ISS zarya [31] on 11-4-2020 at time 5:19:50 is given by,

```
1 25544U 98067A 20102.22211638 .00001877 00000-0 42676-4 0 9992
2 25544 51.6441 319.8604 0003740 104.4166 46.6925 15.48685017221631
```

The TLE is changed continuously with time and the updating of TLE is done regularly by NORAD TLE database [31]. This updates make the TLE very precise for the prediction. If we want to find the position of ISS Zarya satellite on 13-4-2020 and time 5:20:30, the model takes the input of these parameters and output will be in Phase points in ECI. The Phase point at that particular time and data are as follows, In the table 1, the results are in

Table 1: Phase points in ECI frame for ISS zarya

Components	Position	Velocity
x	-2307.602	-5.546
y	5869.336	0.107
z	2527.379	-5.288

km unit. From the results, the x and z components of velocity are -5.546 and -5.288 km per sec. Using the geometry of the reference frame, the angular direction between satellite position vector and vernal equinox vector will be our RA and angular direction between position vector and an equatorial plane or XY plane will give the Declination.

After applying the same concept, the results are given as follows, **RA = 7.431 hours and Dec = 21.838 degrees**. That means vernal equinox direction is 7.431 hours behind the satellite. Suppose we want to measure the elevation or altitude and azimuth angle of the satellite which depends on the observer location, we need to define the latitude and longitude of the observer to find the coordinates. Suppose the current position of the observer is **23.014 latitude and 72.775 longitudes**. The elevation is the angle between the horizon plane made by observer and satellite vector position, and the azimuth is the angle between satellite direction and north direction with respect to the observer. The results are as follows, **Elevation or Altitude = -50.47 and Azimuth = 58.572**.

From the geometry, the multiple parameters are obtained like the distance between satellite and observer, velocity, etc. The simulation of the variations

3 METHODS AND RESULTS

of these results in RA-Dec and Alt-Az is also done by the matplotlib library. Using that the plot between altitude and azimuth angle was obtained and the result is as follows,

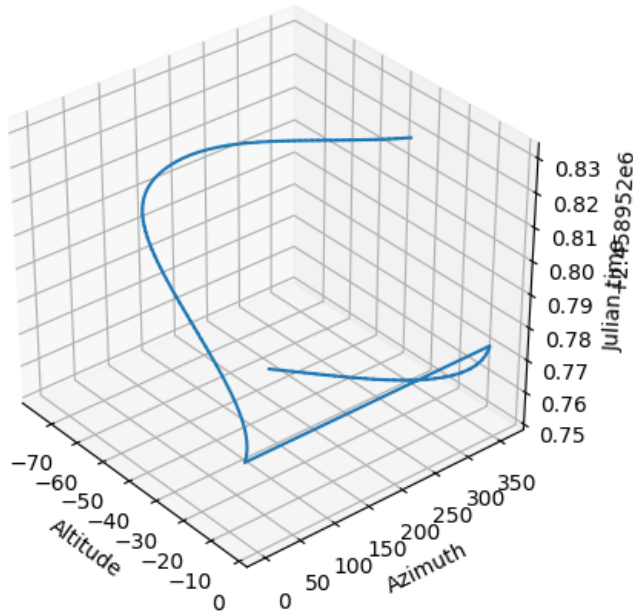


Figure 19: 3D plot of altitude and azimuth angle

The 3D result of altitude and azimuth angle variation of satellite with time (Julian time) is given in figure 19. The time interval between the starting and endpoints of the satellite is taken as 2 hours. That means the trajectory that is given in figure has the starting time 6:0:0 to 7:59:59 on the same date. The variation of azimuth angle is from 0 to 360 degrees while the elevation varies from 0 to around -70 degrees. That trajectory is given in space-time geometry. In the two dimensions, the phase plot is given as follows,

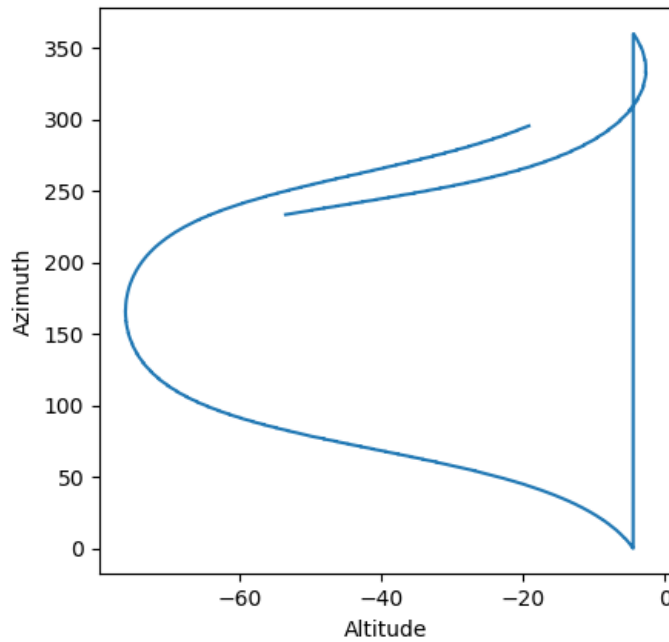


Figure 20: 2D plot of altitude and azimuth angle

The 2D plot is the same as 3D but the time dimension has been omitted. It is apparent that the satellite completes the one cycle of its motion around the earth and goes forward a little bit. The starting point of the satellite and endpoints are not matching very well that is because of the motion of the earth's rotation.

Similarly, the plots for coordinate which is independent of the observer's location are also obtained in Ra-Dec. The 3D profile of satellite trajectory in RA-Dec coordinate system is given below,

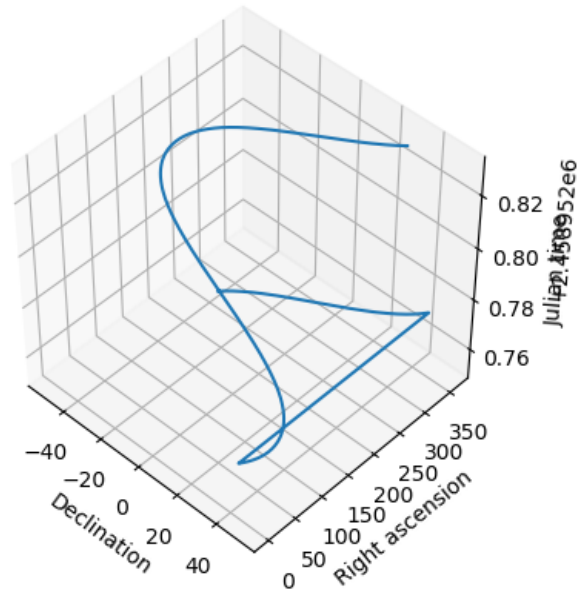


Figure 21: 3D plot of right ascension and declination angle

The trajectory looks same as altitude and azimuth profile. The two dimensional contour is given below,

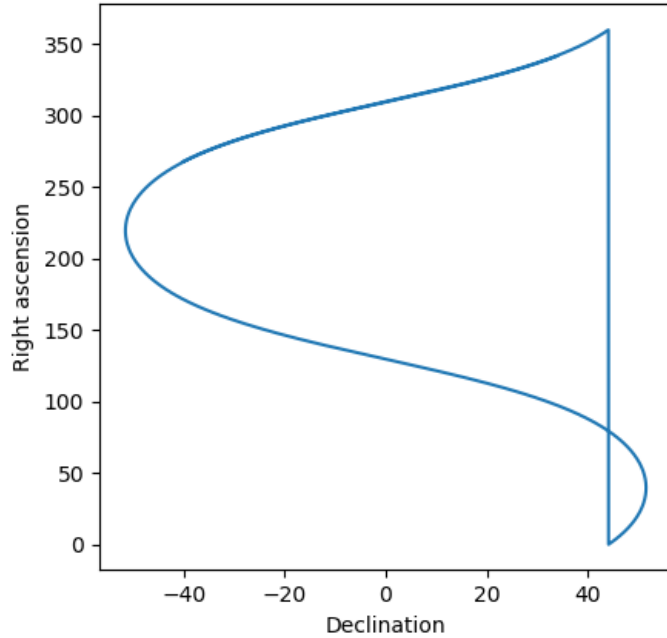


Figure 22: 2D plot of right ascension and declination angle

Here, the shape looks like an infinity shape. Also, the maximum declination of any satellite trajectory will be equal to the inclination of its orbit. Here from the approximation, the maximum declination is around 51.3 degrees which are the inclination of the orbit. This is a low earth orbit satellite which has mean motion around 15 to 10 times. The geostationary satellite has a mean motion around 1 that is why it took 24 hours to complete the whole orbit. We made the trajectory of a geostationary satellite and it came out with very interesting results which are shown below.

The Japanese satellite **Quasi -Zenith Michibiki-1** has been taken as a geostationary satellite which has orbital period time is the same as the earth's rotation period [31]. The TLE of the given satellite is,

```
1 37158U 10045A 20115.95841260 -.00000085 00000-0 00000+0 0 9991
2 37158 41.5769 144.3492 0754668 270.3052 281.7511 1.00289559 35215
```

Here, the epoch time, when the location of the satellite position was measured, is 24-4-2020 at 23:00:07. The result of the data we got on 26-4-2020

3 METHODS AND RESULTS

at 1:30:30. On the particular mentioned date and time, the results are as follows,

Table 2: Phase points in ECI frame for Quasi-Zenith -1

Components	Position	Velocity
x	35189.470	-1.001
y	602.082	2.732
z	-18603.977	-1.450

In table 2, results are in km and it is in the frame of ECI reference. The actual orbital trajectory of the QZS-1 looks like the infinite shaped [37] in the Alt-Az system. The results of the model on 26-4-2020 at 1:30:30 are shown below and it has better agreement with the trajectory.

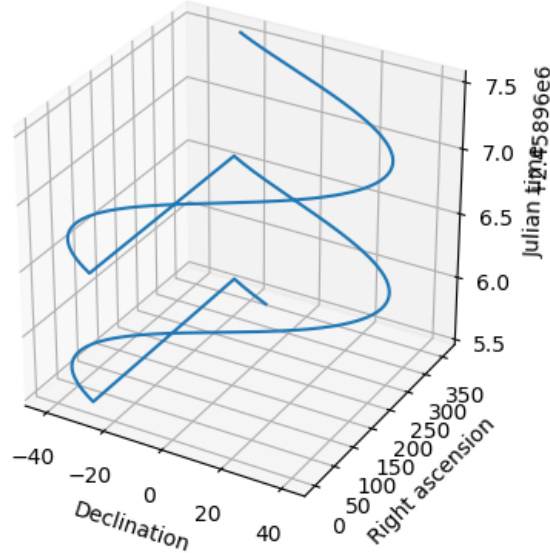


Figure 23: 3D plot of right ascension and declination angle for QZS-1

The QZS-1 moves from -41 to 41 degree with respect to the equator. The

3 METHODS AND RESULTS

above figure is shown in three dimensions and it completes the orbit twice in 48 hours. The 2D projection is given below,

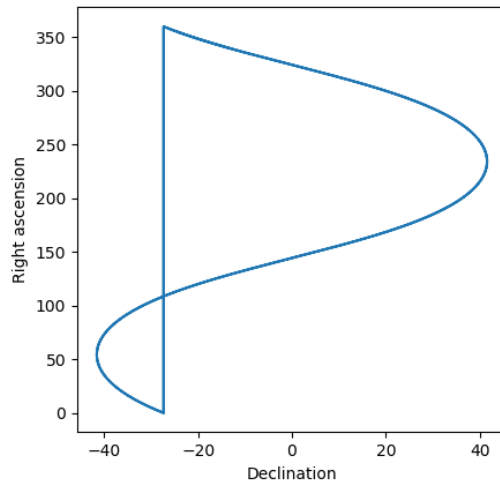


Figure 24: 2D plot of right ascension and declination angle for QZS-1

The shape looks like infinite and also this same result occurs in alt-az profile which is shown below,

3 METHODS AND RESULTS

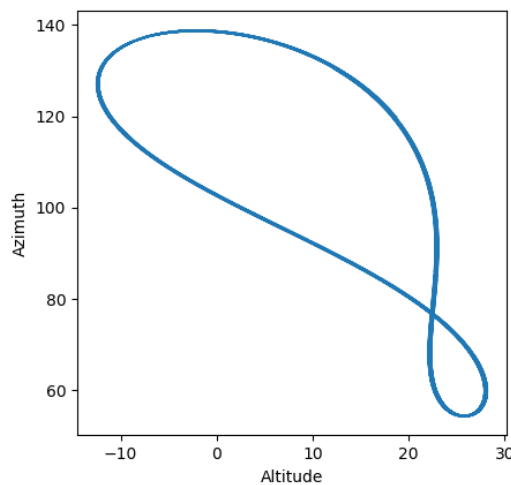


Figure 25: 2D plot of altitude and azimuth angle for QZS-1

The 3D plot is as follows,

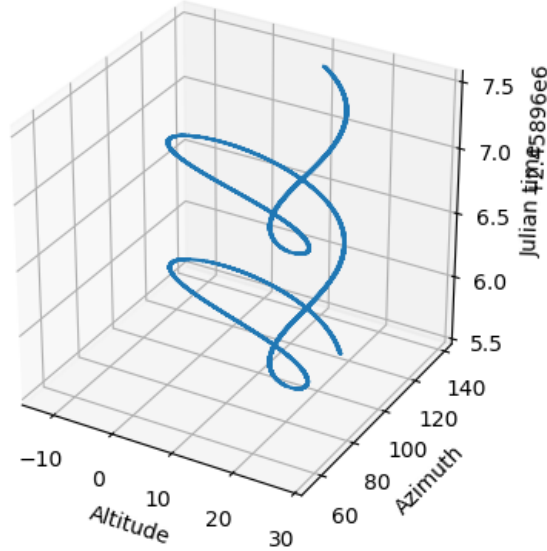


Figure 26: 3D plot of altitude and azimuth angle for QZS-1

This is for geosynchronous or geostationary satellite with time period of 24 hours to complete a orbit at location of latitude 23.0143, and longitude 113.7751.

The Iridium 33 is a debris from the satellite Iridium and it was generated due to the collision between two satellites Iridium and Cosmos in 2009 [38]. Here it is the TLE of a Iridium (one element from the debris) debris,

```
IRIDIUM 33 DEB
1 33772U 97051K 20183.39071590 .00007274 00000-0 62951-3 0 9998
2 33772 86.4017 137.7485 0020735 127.2720 354.3203 14.96847990604358
```

The epoch time (20183.39071590 at third element in TLE), when the TLE was obtained, is on 1-7-2020 at 9:22:37 and the results of the coordinates of position and velocity which are given below, on 2-7-2020 at 5:30:30 UTC using the model. The result of the debris in altitude is 6.00 degrees, azimuth

3 METHODS AND RESULTS

is 140.20 degrees and in right ascension is 8.94 hours and declination is -41.48 degrees.

Table 3: Phase points in ECI frame for Iridium 33

Components	Position	Velocity
x	-3641.539	-3.921
y	3748.279	3.129
z	-4620.171	5.638

The nature of the trajectory of the satellite is given in the below figure,

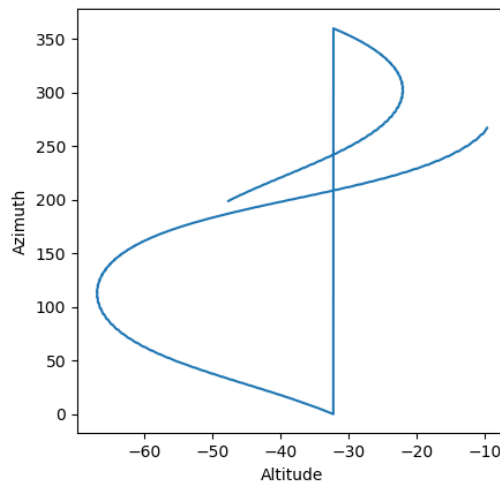


Figure 27: 2D plot of altitude and azimuth angle for Iridium 33

3 METHODS AND RESULTS

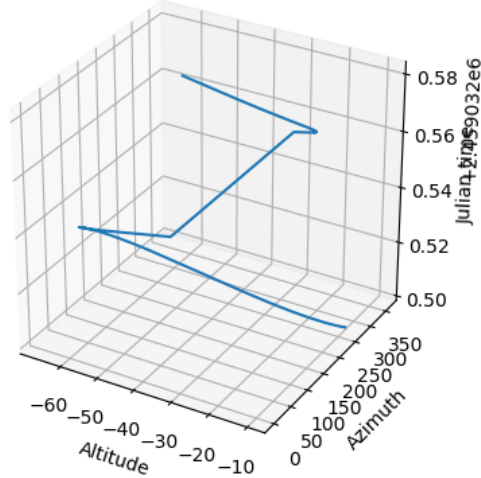


Figure 28: 3D plot of altitude and azimuth angle for Iridium 33

The shape of the profile is very unusual because it is a part of the satellite which was collided. This will make the shape of the orbit very random with high eccentricity. The three dimensions and two dimensions of the right ascension and declination are given below,

3 METHODS AND RESULTS

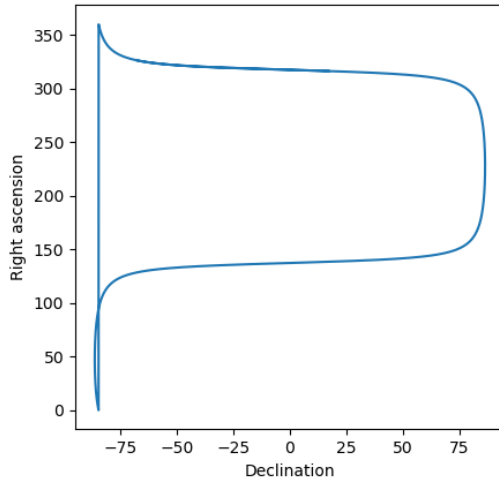


Figure 29: 2D plot of right ascension and declination angle for Iridium 33

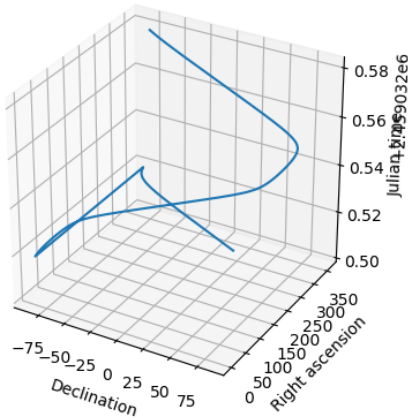


Figure 30: 2D plot of right ascension and declination angle for Iridium 33

The time period of this debris is around 1.7 hours. And the minimum distance between earth and debris is around 780 km. After knowing the position of the satellite with the help of the SGP4 model, the trails simulation

is obtained using the positions of the satellite within the field of view. Now, the next part is the image processing mechanism in CCD and satellite trails simulation. The simulation's results are useful in the algorithm to get precise TLE from the optical observations of the satellite. In the background section, the CCD is explained very well. It is a device for the imaging. But there are noises associated during the simulation. Some of these noises are related to the sky and CCD. The explanation of the different noises during the simulation and its results are shown in below section.

3.2 (2) Simulation of the satellite trails

The simulation of the satellite trails requires tremendous insights into CCD, other factors like atmospheric extinction, point spread function, aliasing effect, and phase angle. The detailed information and results are given in the further sections.

3.2.1 Noises and efficiency of CCD

Noise sources are divided into two parts temporal and spatial. Temporal noise can be reduced by frame averaging, while spatial noise cannot. However, some spatial noise can be removed by frame subtraction or gain/offset correction techniques [10] and [40].

3.2.1.1 Shot noise Shot noise is the photons coming from randomly all over space which is nature's fundamental limit which can't be avoided. This noise is related to the source of the object. The number of photons coming from the source varies with time and follows the Poisson distribution. Since the time between photon arrivals is governed by **Poisson statistics**, the uncertainty in the number of photons collected during a given period of time is simply $\sigma_{shot} = \sqrt{S}$. Here S is signal expressed in photons numbers. So a 10,000-photons exposure will have a shot noise of 100 photons [10] and [40].

The noise associated with the source and this could not be removed very easily. Because this noise follows the Poisson distribution. Even the source has photon flux around 100, it would have noise approximately 10 photons. That means the temperature of CCD, exposure time, area of the telescope could not remove this particular noise.

3.2.1.2 Reset noise By sensing the capacitor, we can find the voltage domain of collected charged packets from each pixel. Before measuring each pixel's charge packet, the CCD's sense capacitor is reset to some reference level. There is an uncertainty in this voltage related to thermal noise generated by the channel resistance. It is given by $\sigma_{reset} = \sqrt{4kTBR}$. Where k is Boltzmann constant, T is temperature, B is the noise power bandwidth (Hz), R is the resistance. It is also expressed in $\sigma_{reset} = \frac{\sqrt{kTC}}{q}$. Here C is the capacitance of sense and q is a fundamental charge. Most manufacturers of CCD cameras include circuitry that completely eliminates it. R is the effective resistance and it is around 350 ohm. With a bandwidth of 1 MHz and temperature at $T = 193K$, the reset noise in V/rtHz is $1.9314 \cdot 10^{-6}$. The bandwidth is the frequency at which the imaging is done with that rate. Also, the RMS value is obtained by dividing the value through sensitivity. The sensitivity is the main factor to convert this unit to RMS electrons. The sensitivity is around 10^{-6} for the standard CCD and the final reset noise in RMS electron will be around 2 per pixel [10] and [40].

3.2.1.3 White noise This is readout noise at the output of the amplifier. The output amplifier has resistance and noise is associated with this resistance and the temperature. The effective resistance, in this case, is the output impedance of the source, R_{out} . This type of thermal noise is sometimes called ‘Johnson noise’. It is represented by $\sigma_{white} = \sqrt{4kTBR_{out}}$. The unit of this noise is V/rtHz and it is converted to RMS electrons by dividing sensitivity. The value of k is taken in J/K unit and bandwidth is taken normally as 1000000 Hz from the standard CCD iKon-M 934 Series. The R is the resistance of the output channel of the CCD. It is taken as 2000Ω . T is 193 K and after all these values the σ_{white} is $4.617 \cdot 10^{-6}$ V/rtHz. Considering the sensitivity 10^{-6} , the RMS electrons of this noise is 4.617 RMS electrons per pixel [10] and [40].

3.2.1.4 Flicker noise This noise is dependent on the inverse of frequency f . Higher the frequency, lower the noise in the image. The noise power is given by $\frac{V^2}{Hz}$ and it is decreased by 10 factors with each decade increase in frequency. It is caused by surface and bulk traps of electrons due to defects and contaminants that randomly capture and release carriers. Many natural systems exhibit $1/f$ behavior. They have in common a collection of states that turn on and off individually with randomly distributed time

constants. Generally, the approximate value of the flicker noise is around $100 \cdot 10^{-9}$ V/rtHz at low temperature. The unit is V/rtHz and to convert into electrons, the sensitivity of the CCD plays a role. Dividing sensitivity to V/rtHz (flicker noise), the unit conversion would be in RMS electrons per pixel. Also, the flicker noise follows the Gaussian or Normal distribution. After taking sensitivity as 10^{-6} , the final answer in RMS electrons would be 0.10 per pixel [10] and [40].

3.2.1.5 Clocking noise A number of clocking circuits are required to accumulate and process the signal from input to output. The noise is associated with the output waveform called clocking noise due to the circuits. It is dependent on the square root of clocking frequency. The clocking noise is not considered because it is very less compared to other noise.

These reset noise, white noise, flicker noise, and clocking noise come into readout noise. Because these noises are produced during the reading of the image. It is because of the resistance and frequency of reading and in this process, some of the electrons escape from the channel. The readout noise is the sum of these noises. Therefore readout noise is equal to white noise + reset noise + clocking noise + flicker noise. The reason behind the independency of these noise from the exposure time is because these noises are generated during the reading of the image as the name suggests. Therefore, after some time or after exposure time when the image is ready to read, the processor takes each pixel voltage and converts into digital form with a certain frequency. And during this process, the readout noise will be generated.

As mentioned before, these noises are dependent on the bandwidth of the frequency, resistance in the channels, and temperature. After dividing the noise by sensitivity, the final output would be in RMS e-. These noises follow the normal distribution and the output of RMS value would become the standard deviation of the normal distribution with a mean value of zero [10] and [40].

This variations in table 4 are at 1 MHz frequency bandwidth in the CCD. The rate of the variation with temperature is decreasing with temperature. Because the read noise mostly depends on the square root of temperature.

In table 5, the noise becomes very large at 100 MHz frequency bandwidth. This noise still around 70 RMS e- per pixel at T = 193 K. In the imaging process, the temperature doesn't change very much but bandwidth does. The

Table 4: Read out noise's variation with temperature in 1024 x 1024 pixels CCD (1 MHz)

Temperature (K)	Read out noise (rms per pixel)
193	7.0255
233	7.7094
273	8.3368
303	8.7775

Table 5: Read out noise's variation with temperature in 1024 x 1024 pixels CCD (100 MHz)

Temperature (K)	Read out noise (rms per pixel)
193	69.3558
233	76.1949
273	82.4681
303	86.8759

readout noise is verified with [41] at temperature 193 K.

3.2.1.6 Dark current Dark current is the result of imperfections or impurities in the depleted bulk silicon or at the silicon-silicon dioxide interface. These sites introduce electronic states in the forbidden gap which act as steps between the valence and conduction bands, providing a path for valence electrons to sneak into the conduction band, adding to the signal measured in the pixel. Because of the imperfections, the small thermal agitation could jump the electron easily. The dark current is generated because of thermal fluctuations. Therefore, CCD is placed in a very cooled place to avoid this noise addition. There is other two noise related to surface and bulk [10] and [40]. These noises are generated because of carelessness in the manufacturing of its surface.

Therefore, the dark current is given by,

$$Dn = 2.5 \cdot 10^{15} \cdot A \cdot I \cdot T^{1.5} \cdot e^{-\frac{E}{2kT}} \quad (3)$$

The unit of the Dn is electrons/pixel/second. The T is variable temperature surrounding the CCD. A is the area of a pixel in cm^2 and I is a dark current at temperature 300 K. It changes with quality of the CCD's. In general, the value of I lies between 0 to 2 nanoamperes/cm/cm. But in the model,

3 METHODS AND RESULTS

the value is taken as 0.018. Also k is the boltzmann constant in eV/K. Finally, the E is the band gap energy in silicon diode which also varies with temperature. These reference values are taken from standard CCD iKon-M 934 [41]. E is defined by,

$$E = 1.1557 - \frac{7.021 \cdot 10^{-4} \cdot T^2}{1108 + T}$$

The E is in the eV unit. After considering all the values of these variables and constants for standard CCD like iKon-M 934 Series, the values are given as follows, $T = 193$ K, $I = 0.018$ nanoamperes/cm/cm, $A = 169$ square micron, $k = 8.6173 \cdot 10^{-5}$ eV/K. After putting all these numbers into equation 3, the Dn is 0.0003038 e-/pixel/second [41].

To find the total dark noise using dark current, the multiplication operation of time and number of pixels is done with Dn . The time represents as exposure time. Thus, the more the exposure time, the more the dark noise which varies with linearly. Also, the variation of the dark noise with temperature is very obvious from the intuition. It is a fact that the temperature rise would increase the dark noise. The dark noise increases with exposure time. In the below figures, the time is taken as variable t between 0 to 1000 s.

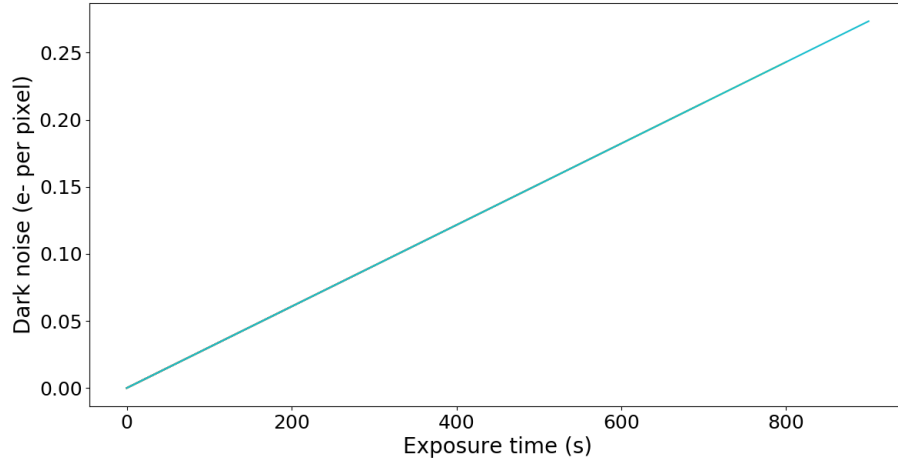


Figure 31: Dark noise at $T = 193$ K

From figure 31, the dark noise increases with time in a linear fashion. Because noise is proportional to the time directly. The unit of the noise is e-

3 METHODS AND RESULTS

per pixel. From the figure, the output electron at temperature $T = 193$ K, the noise is negligible and the maximum noise at $t = 1000$ s is around 0.27 e- per pixel.

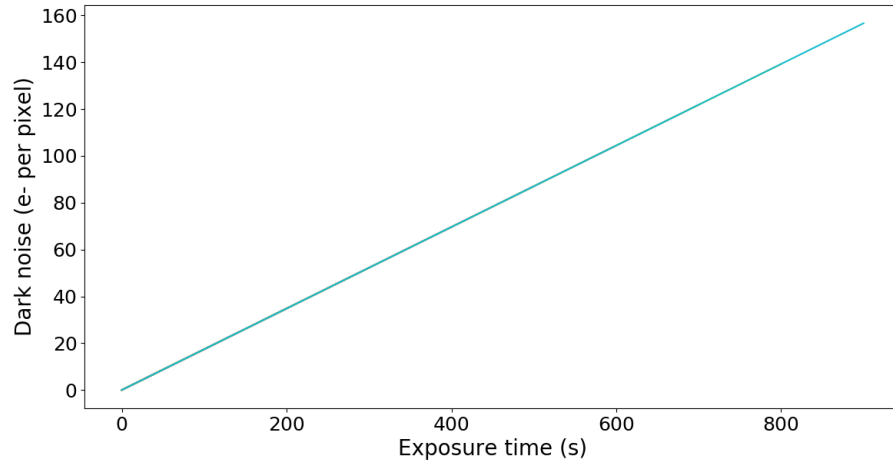


Figure 32: Dark noise at $T = 233$ K

Here also, the variation is proportional to time at temperature $T = 233K$ and the maximum value is 160 e- per pixel which is not negligible. It could affect the quality of the image.

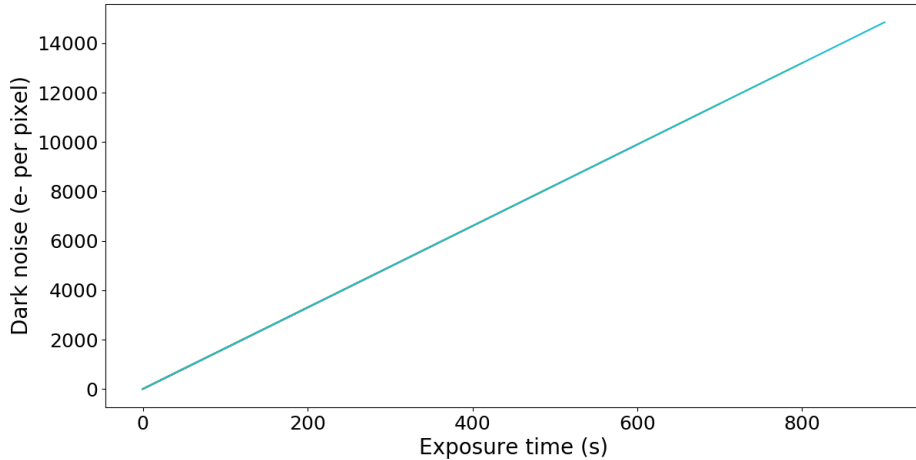


Figure 33: Dark noise at $T = 273$ K

In the above figure, the maximum value is 14000 and that is very large noise and could dominate the point image. Therefore, temperature $T = 273$ K is not desirable and feasible. To avoid this noise, the CCD is kept at a very low temperature at around 190 to 230 K. The cooling process slow down the thermal fluctuations inside the sensor. All the results are verified with [41].

3.2.1.7 Sky background noise The noises from other stars or any interference like light, the bulb could affect the image quality. Still, the image can't get rid of the sky noise from different stars and celestial bodies. It is randomly and follows the Poisson distribution. The sky background is given in the unit of mag/arcsec-2. But the brightness or intensity of an object is given by magnitude if it is a point image. This kind of point source has the only magnitude because the telescope cannot resolve the surface of the distant stars. It is similar to a satellite. Satellite's brightness is given in magnitude. But for the extended source which has an apparent surface, its brightness is given in mag/arcsec-2. Thus, the field of view will decide how many photons will fall on the CCD randomly. Another parameter, time exposure will also essential to consider. If the field of view and exposure time are high then noise contribution from the sky would be very high. Generally, the sky brightness has a value of around 21 mag/arcsec-2 in visible range [42].

3 METHODS AND RESULTS

Therefore, around 600 ADU will be assigned to each pixel if the exposure time is 1s, and the field of view is in 180 X 180 arc second. The formula of the sky background noise is given by [42],

$$n_{sky} = f_v^2 \cdot \pi \cdot 10^{-0.4 \cdot m_v} \cdot 8.8 \cdot 10^9 \cdot QE \cdot t \cdot D^2 \cdot \pi \quad (4)$$

In the above equation 4, the QE is the quantum efficiency of the CCD and D is the diameter of the telescope aperture. f_v^2 is the square of the field of view of the CCD and m_v is the magnitude of the sky. The quantum efficiency and magnitude is explained in further sections. The field of view has arc-sec unit and diameter of the aperture in meters. The n_{sky} is total sky noise within the field of view. Therefore, to calculate the noise per pixel, the output is divided by a total number of pixels to get the average number. Also, this noise follows the Poisson distribution.

Suppose, the field of view $f_v = 180$ arc-sec with sky background apparent magnitude $m_v = 21$ magnitude/arc-sec² is given in the model. Also, the $D = 1.2$ m, $QE = 60\%$, and exposure time $t = 1$ s are taken as standard values. The sky background incoming photon numbers would be 966942659.85. This value is spread over the all pixels and illuminates them. To calculate the average value of photons per pixel, the value is divided by total number pixels. For example, in 1024 x 1024 CCD, the average number is 922 photons. The associated ADU is 600 in gray scale [42]. The ADU is the digital unit for the image and it is described in the further sections.



Figure 34: Images with sky background noise and without noise

3 METHODS AND RESULTS

There are many techniques to remove noise. For example, to remove the sky background noise, one blank frame of image is taken to measure the noise with a particular time and field of view. After subtracting this frame from the real image, it would eradicate the noise.

The signal to noise ratio is the last thing that should be taken care because the more the signal to noise (SNR) is, the more the signal would be strong. The SNR is dependent on read out noise, dark noise, sky noise, shot noise. After the calculations, the dependency of SNR is given below [10] and [43],

$$SNR = \frac{S_0 \cdot Qt}{\sqrt{S_0 \cdot Qt + S_s \cdot Qt n_p + S_d \cdot tn_p + R^2 n_p}} \quad (5)$$

In the equation, S_0 , S_s , S_d , R are noise related to shot, sky, dark and read out, respectively. Q , t , n_p are quantum efficiency, exposure time, and number pixels spread by object or point source.

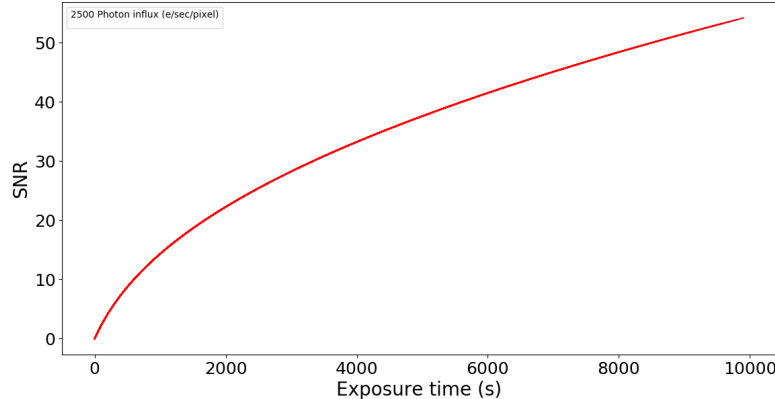


Figure 35: Signal to noise ratio for 2500 electrons per pixel per second

The SNR increases with exposure time in parabolic fashion. It varies with quadratic nature and for infinite exposure time the SNR would be saturated at one point [43]. But the exposure time increases the strength of the signal as it is visible from figure 35

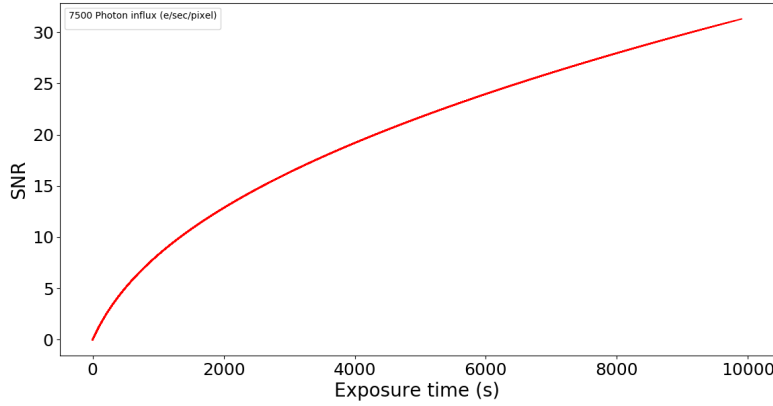


Figure 36: Signal to noise ratio for 7500 electrons per pixel per second

Also, the difference between figure 36 and 35 is that photon flux on a pixel. Figure 35 has 2500 photons flux while figure 36 has 7500 photons flux. But for 7500 photon flux, the SNR is lower than 2500 photon flux. The higher the photon flux, the less the SNR and signal would be weak. SNR is essential to calculate and analyze the image quality [10] and [43]. Now the noises related to source and CCD have been found using certain mathematical equations but the gray value of a pixel is determined by flux of the photons and satellite's magnitude and extinction. Next section describes the magnitude and satellite trails details.

3.2.2 Magnitude of satellite and its phase angle

TLE data has come from the observation of space debris using a ground telescope. It uses high-quality CCD for the measurement. Its magnitude plays a role to find distance and its variation with time and position. From that, velocity could be found and its related parameters. It is also useful to remove space debris trails from pictures for analyzing. The brightness or apparent magnitude of satellites comes from sunlight. Sunlight incident on the satellite's material like solar plates or ceramics etc. After reflection of the incident light, it will come to an observer on the earth. But before that, light passes through the atmosphere of the earth and loses its brightness due to scattering and absorption. The next section describes the attenuation of the apparent magnitude of the satellite using various equations. The brightness

3 METHODS AND RESULTS

of the satellite depends on different parameters like albedo (reflectivity), area, distance, phase angle, and magnitude of sun [21]. The terms are explained below,

The absolute magnitude of any celestial object is the apparent magnitude of that object when it is far from the observer at 10 parsec distance. 1 parsec is equivalent to $3.1 \cdot 10^{13}$ km. An apparent magnitude is the magnitude value of the object when it is observed from earth. The magnitude is equivalent to the brightness of the star or object but in the reverse scale. If the brightness of the object is more then the magnitude would be less. The magnitude of the star follows the blackbody radiation but here in satellites and debris, they are illuminated by sunlight. The sunlight reflection depends on the surface of the debris or satellite. The reflection is defined by the albedo of the material. In the parameters, albedo is the ratio between reflected light and incident light. It varies with wavelength. Moon has 0.12 albedo value in visual range of wavelength [44] and [45]. ISS (Zarya) has 0.6 to 0.7 because of solar panels. The area is the cross-section area of the object when observed from the earth. Generally for satellites, it is assumed to be a spherical shape with a certain radius. The phase angle is the angle between sun to satellite direction and satellite to observer direction. It is shown in the below figure,

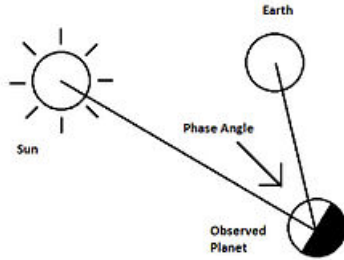


Figure 37: Phase angle of satellite

When the phase angle is zero, the moon will be at the full moon phase. Magnitude changes with phase angle. At the 90 phase angle, the moon would be at the first quarter phase. Magnitude is a kind of scale to describe the brightness. Brightness and magnitude have logarithmic relation, therefore high brightness star would have a negative or minimum value of magnitude. As the magnitude increases, the brightness will be decreased [46].

3 METHODS AND RESULTS

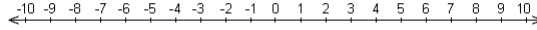


Figure 38: Magnitude scale

As mentioned above, the scale appears to work 'in reverse', with objects with a negative magnitude being brighter than those with a positive magnitude. The more negative the value is, the brighter the object. The absolute magnitude is measured with reference to brightest star Vega. Apparent magnitude is assumed to be zero for Vega star for the reference. With reference to that, Sun has -26.74 apparent magnitude and 4.83 absolute magnitude. Moon has apparent magnitude of -12.6 [46]. ISS satellite has minimum -6 apparent magnitude.

$$m_2 - m_1 = -2.5 \cdot \log_{10} \left[\frac{b_2}{b_1} \right] \quad (6)$$

In the equation 6, the m_2, m_1 are apparent magnitude of star 2 and 1, respectively. Similarly, b_2, b_1 are apparent brightness of them [46]. When comparing apparent and absolute magnitude of a star, we get the distance modulus and it is given by,

$$m - M = 5 \cdot \log_{10} [d - 5] \quad (7)$$

Here m, M are apparent and absolute magnitude of a star and d is the distance between star and observer in parsec. Also, brightness and luminosity is related by $B = \frac{L}{4\pi d^2}$ [47].

The apparent magnitude of satellite is defined by various equations. The reflection of the light could be specular or diffusive. Based on that there are various formulas. The general formula is given by [21],

$$m = -26.58 - 2.5 \cdot \log \left[\frac{A\gamma F(\phi)}{R^2} \right] \quad (8)$$

A is the cross-section area of satellite when it is observed from earth. γ is albedo or reflectivity of satellite's material. R is the distance between satellite and observer. $F(\phi)$ is the function of phase angle. The phase angle is defined by [21],

$$\cos(\theta) = \frac{|r_{sat} - r_{obs}|^2 + |r_{sun} - r_{sat}|^2 - |r_{sun} - r_{obs}|^2}{2 \cdot (|r_{sat} - r_{obs}|)(|r_{sun} - r_{sat}|)} \quad (9)$$

3 METHODS AND RESULTS

θ is phase angle and $r_{sat}, r_{sun}, r_{obs}$ are position of satellite, sun, and observer, respectively in same coordinate system of ECI. In the equation 8, -26.58 is apparent magnitude of sun. $F(\phi)$ varies with shape of satellite and its surface. For example, satellite is a sphere with diffusive reflection then $F(\phi)$ is given by $F(\phi) = \frac{2}{3\pi^2} \cdot [(\pi - \phi)\cos(\phi) + \sin(\phi)]$, where ϕ is in radian. If satellite has specular reflection surface then $F(\phi) = \frac{1}{4\pi}$ [48]. Here apparent magnitude of satellite m is without earth's atmosphere. We need to take consideration of atmospheric extinction which scatter or absorb the light during its path. Atmospheric extinction is given in next section.

Here the phase angle is very important. Even in the moon's phases, it is due to the phase angle. The earth blocks a little bit portion of the moon to illuminate it. And we see the phases of the moon. Similarly, the satellite's magnitude changes with phases. The phase angle θ is defined in the equation 9 [48]. From the equation, it is apparent that the phase angle is dependent on the distances between earth and sun. Also, the magnitude of the satellite depends on albedo, surface area, and distance between observer and satellite. Albedo depends on surface properties. Basically, the satellite is powered by solar plates and these plates have good reflective because of the glass. The surface area also plays a role in the magnitude. The higher the area, the more the apparent magnitude. And the last one is distance. If the distance is very large then the magnitude would be attenuated with distance. This will decrease the magnitude.

But the phase angle is very crucial to observe the satellite. Because with time, the phase angle changes and the apparent magnitude. Sometimes, satellite totally become invisible if the phase angle is not beyond a certain value. Before calculating the phase angle, the sun's position is very important to calculate the distances. For the moon, 0 degrees is the position when the moon is on the opposite side of the earth during the night. Because of that, we don't see the moon. That phase is the new moon phase. Moon takes around 28 days to rotate around the earth. Therefore, the phase angle changes with the time period of 28 days. After certain days, the moon comes in such a phase that, it appears only half of it. This position has a phase angle of 90 degrees. And at 180 phase, the phase is a full moon when the moon appears to be full. Because the sun-light totally incidents on the whole surface of the moon and illuminates it [49]. The albedo of the moon is around 0.2. The phases of the moon are given below,

3 METHODS AND RESULTS

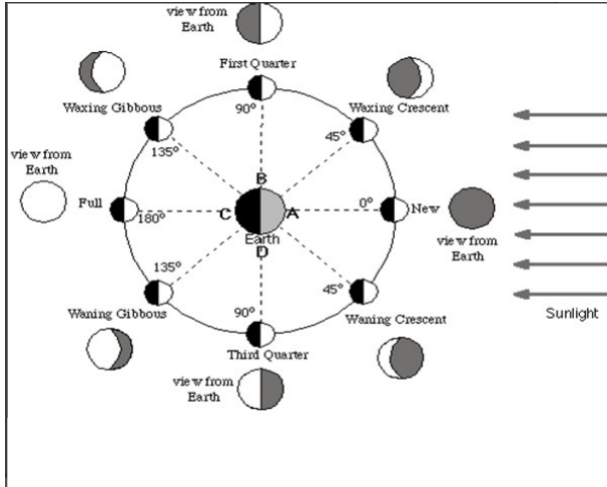


Figure 39: Moon's phases

In the above section, the three satellites have been taken for finding the position. Here, the phase angle of these satellites has been given below with some assumptions of its size and albedo.

3.2.3 Results of phase angle and magnitude

(1) ISS (Zarya) As mentioned about the ISS satellite's TLE and its position with time, it has a size of around 12.5 m X 4.1 m in length and diameter [50]. Therefore the average size of the satellite is taken as 10 meters to calculate the surface area of the circular disk if we assume the satellite a sphere. The albedo of the satellite is around 0.75 and distance is variable which changes with time. Mostly, the orbit of this satellite is almost circular with less eccentricity. Thus, the distance would be around 420 km [50]. After incorporating all these values, the apparent magnitude and phase angle are found as shown in the below figures.

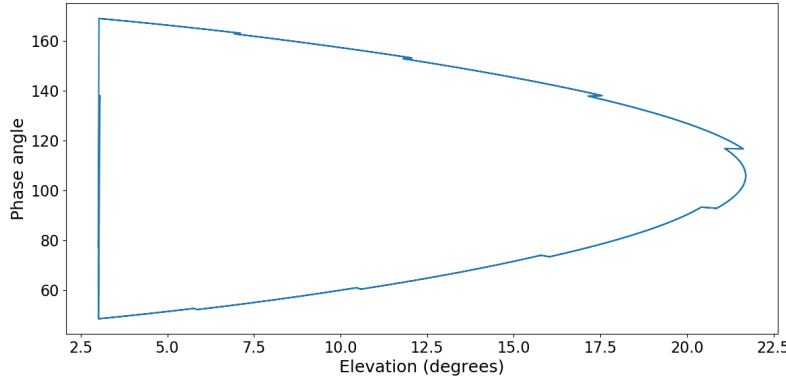


Figure 40: The variation of phase angle with an elevation of ISS satellite

In the above figure, the phase angle is started from 55 degrees to 170 degrees. The maximum value of the elevation is 22.5 degrees on 30-4-2020 at the location of 23 latitudes and 72.7 longitudes. Also, the maximum apparent magnitude is around 6 and a minimum at -2.5. From the observation, at 170 phase angle, which is maximum, has apparent magnitude -2.5. It is also verified that the ISS satellite has a minimum -3 apparent magnitude from the shortest distance at 180 phase angle. The satellite starts dimming as the elevation of the satellite increases. This increment changes the phase angle and the magnitude. At last, when the phase angle becomes around 55, the magnitude becomes around 5 to 6 which is very hard to notice with the naked eye.

3 METHODS AND RESULTS

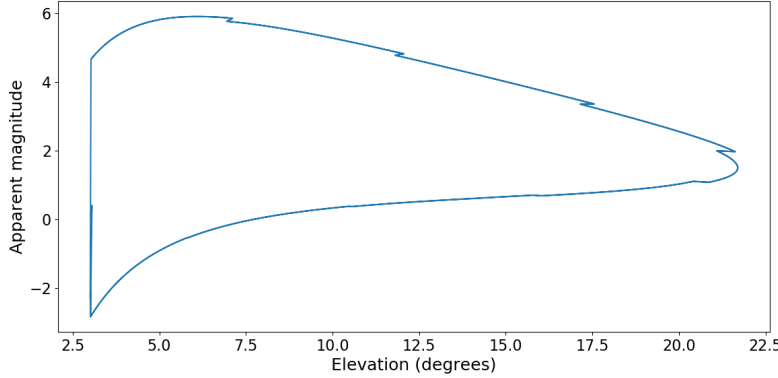


Figure 41: The variation of apparent magnitude with an elevation of ISS satellite

Another result of the Iridium 33 is shown in the below figure. The size of the debris is taken around 5 to 10 cm with 0.3 albedo value [38]. The trend looks very randomly and the debris passed through the location at 23.0143, 72.7751. The maximum angle of the elevation is 25 degrees with a phase angle at 90. The curve with maximum elevation has a minimum phase angle at 40 and ends at 120. Again, the sun plays the main role in the illumination of any objects.

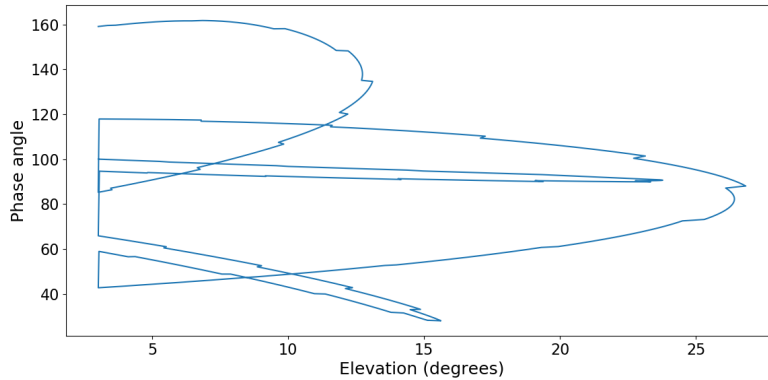


Figure 42: The variation of phase angle with an elevation of Iridium 33

After observing the phase angle of the debris, the apparent magnitude is

the main factor to analyze that its visibility to the naked eye. If the apparent magnitude is greater than 6 to 7 then it is not visible with our eyes.

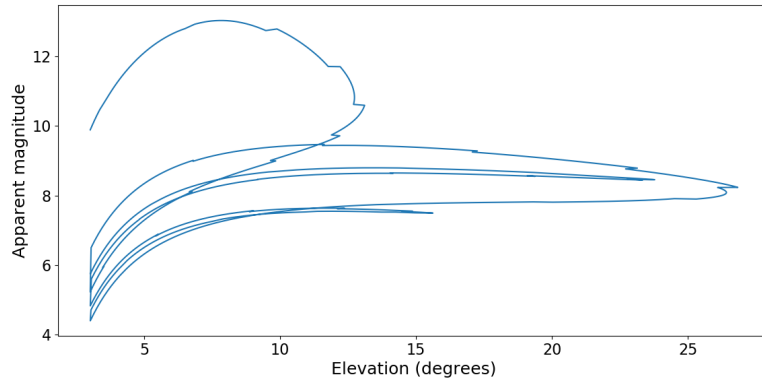


Figure 43: The variation of apparent magnitude with an elevation of Iridium 33

It is assumed that the debris has a size of 50 cm with 0.5 albedo value. Sometimes, it could have 0.2 albedo with a size of 10 to 5 cm. Debris is very small that it is hard to discernible due to turbulence and atmospheric extinction of the atmosphere [38]. From figure 43, the maximum apparent magnitude is at 12 at an elevation of 15 degrees. The minimum apparent magnitude is 3 to 4 at an elevation of 4 to 5 degrees. The trends follow the same behavior as a phase angle. Here, the average distance is around 780 km. This magnitude is attenuated by the atmosphere through scattering and absorption which are described in the next section.

3.2.4 Atmospheric extinction

As the light makes its way through the Earth's atmosphere, some photons collide with atoms, molecules, water droplets, grains of dust, and other objects. These photons may be absorbed by the objects or they may be scattered in a different direction. Either way, they would no longer reach the observer on the ground. As a result, the observer detects fewer light rays from the star than he would have seen on an air-free planet. We call this dimming of stellar light extinction. The extinction depends on the distance in the atmosphere light traveled [23]. It is described by airmass.

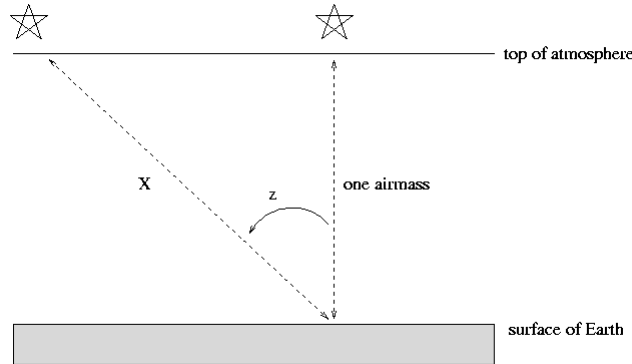


Figure 44: Airmass and zenith angle

Target is some angular distance away from the zenith, indicated by the zenith angle z in the diagram above, then its light travels a longer distance through the Earth's atmosphere before it can reach you [23]. Airmass is defined by the below equation,

$$\text{airmass } X = \sec(z) \quad (10)$$

This extinction would decrease the apparent magnitude of star or satellite we observe [23]. It is very essential to consider the extinction factor. The linear relation (Bouguer's law) between magnitude and atmospheric extinction is given by [23],

$$m(X) = m_0 + k \cdot X \quad (11)$$

Here k is the atmospheric extinction coefficient. m_0 is the apparent magnitude of an object without the earth's atmosphere. In astronomy, different band filters are used for observation of objects. The reason behind filters is to analyze its components of the object, for example, certain H- alpha lines, etc. These different band filters have a certain wavelength range. There are so many filters like U, V, R, G, I, B, etc. V is a visual band filter with a wavelength range of 500 to 700 nm. R, G, and B stand for red, green, and blue, respectively. On average, the V band has an extinction constant value of around 0.2 mag/airmass. U has 0.6 higher than any others because of the ozone layer. So different band filters are used for various observations with less extinction [51]. Mostly, the photometry system is used for the measurement of atmospheric extinction. It is very dynamic with spatially and temporally. Second-order extinction is also introduced because of ozone and

3 METHODS AND RESULTS

aerosol scattering.

In the atmosphere, Rayleigh scattering has occurred in a large amount than ozone and aerosol scattering. Total extinction is given by below formula,

$$k_T = k_r + k_o + k_a \quad (12)$$

In the equation 12, k_r , k_o , k_a are due to rayleigh, ozone, and aerosol, respectively. Here k_o is independent on an altitude of the observer because the observer's range is in range of 0 - 1 km. Thus, no matter where we are, the ozone layer would extinct the light from the object at around 15 km. The value of total extinction is found by theoretical formulas or observation [23]-[24]. In the observation, a reference star or standard star is taken. At different airmass, apparent magnitude is measured and profile between magnitude and airmass has been done. The slope of that curve gives the value of extinction at that position and time [23]. If it is linear in behavior, then it is expressed as,

$$k_T = \frac{m1 - m0}{X1 - X0} \quad (13)$$

Equation 13 represents the slope of the curve where measurements are taken at $X1$, $X0$ airmass position with magnitude value of $m1$, $m0$ [23].

There are numerous equation for atmospheric extinction. In the 1999, V. mohan [52] had given set of equations for rayleigh, ozone, and aerosol scattering. The set of equations are given below,

$$k_r(\lambda, h) = \frac{0.0095 \cdot e^{-\frac{h}{8}} \cdot \left[0.23465 + \frac{107.6}{146-\lambda^2} + \frac{0.93161}{41-\lambda^2} \right]}{\lambda^4} \quad (14)$$

$$k_a(\lambda, h) = 0.087 \cdot \frac{e^{-\frac{h}{1.5}}}{\lambda^{0.8}} \quad (15)$$

$$k_o(\lambda) = 839.4375 \cdot e^{-131(\lambda-0.26)} + 0.0381562 \cdot e^{-188(\lambda-0.59)^2} \quad (16)$$

Here h is altitude of observer in km. λ is in μm . Assumptions are taken here to simplify these equations like pressure and molecular density of air. The contribution of ozone scattering is large in wavelength around 590 nm.

The general formula for Rayleigh depends on molecular density, altitude, wavelength, and pressure. Aerosol extinction depends on the aerosol optical depth and altitude. Ozone extinction only depends on the concentration of it in the dobson unit. The general forms are given by,

$$k_r(\lambda, P, h) = \frac{2.5A \cdot \lambda^{-(B+C\lambda+\frac{D}{\lambda})} P}{\ln(10)g(h)M} \quad (17)$$

3 METHODS AND RESULTS

$g(h)$ is equivalent to the acceleration of gravity, P is pressure, and M is the molecular mass of dry air.

$$k_a(\lambda) = \tau \cdot \lambda^a \quad (18)$$

a is an exponent of λ , τ is the aerosol optical depth which depends on the altitude of the site.

$$k_o(\lambda) = I_o \cdot P_o(\lambda) \quad (19)$$

$P_o(\lambda)$ is ozone extinction template from MODTRAN library. I_o is the scale factor expressed in Dobson units. These parameters vary with the location of the observer and the atmosphere's characteristics [52]. Whenever the light comes from the star or any object, atmospheric extinction decreases the magnitude and it plays a very vital role for calculations of photons. The reduction of the apparent magnitude is calculated using considering the below parameters, the height h is assumed to be 0.018 km. The height represents the height of the sensor from the ocean level. Another variable is the λ which is the incident color property of source or satellite in the equations 14 to 16. The extinction is varied accordingly to the wavelength. The variation is given below,

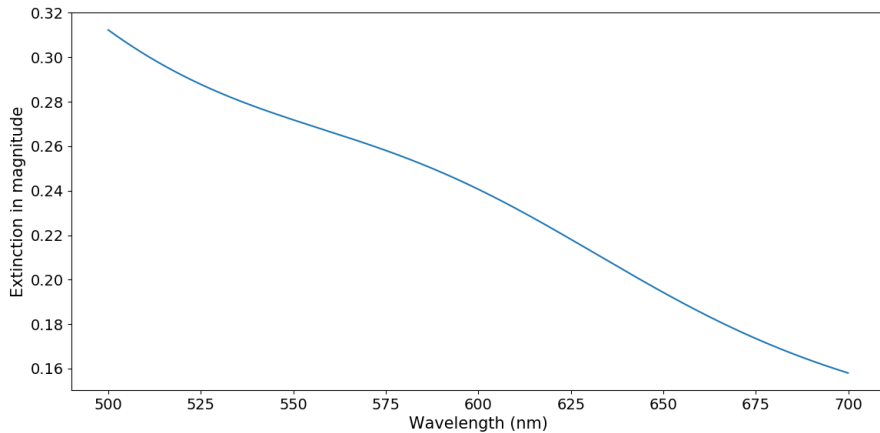


Figure 45: Atmospheric extinction variation with wavelength at $h = 0.018$ km

In the figure, it is apparent that the apparent magnitude of the satellite is decreased with increment of the wavelength. That means, the scattering

3 METHODS AND RESULTS

or absorption occurs mainly at a higher wavelength range. There is a bulge type shape in a range of 530 to 650 nm wavelength. That is because of the ozone layer absorbs or scatters the UV range wavelength. 530 to 650 nm don't lie in the UV range, therefore, the scattering or absorption would be less. And the apparent magnitude is higher than other wavelengths. This variation is only for height at 0.018 km. Also, the maximum extinction is around 0.32, and the minimum is 0.16. That is a very large number in terms of photon numbers.

That is the reason behind the location of the observatories in the mountains or high altitude. Because at high altitude, the extinction would be less and light doesn't need to pass through the troposphere. The below figure is describing the extinction at an altitude of 8 km.

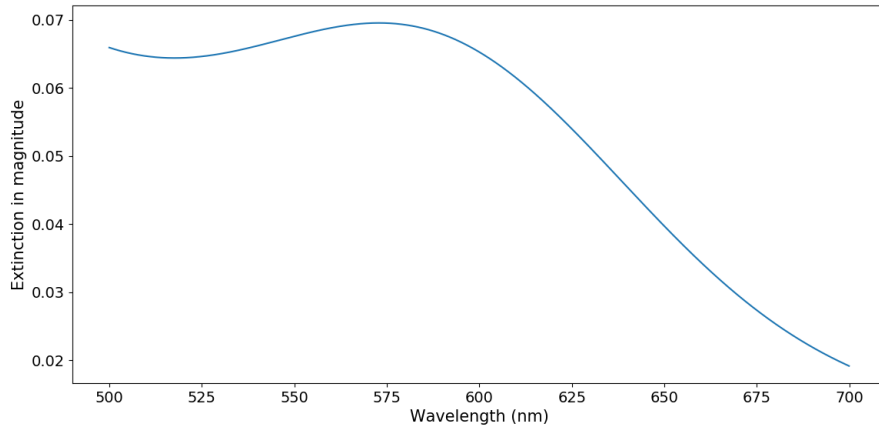


Figure 46: Atmospheric extinction variation with wavelength at $h = 8$ km

From the image, it is visible that the maximum magnitude is around 0.07 and the minimum is 0.02. That is negligible compared to ground level extinction. After the extinction, the satellite's point image is very important to consider in the simulation. This point image is followed the Gaussian distribution around the center. The below section describes the role of point spread function.

3.2.5 Point source function

The image of the satellite from the earth looks like a point. Within a certain field of view in the sky, the satellite only illuminates certain pixels on the CCD. The point images are projected onto CCD in a different way. It follows certain distributions like Gaussian around the point in two dimensions. The point images are described by point spread function [53]. Before the point spread function, why the point image looks like a Gaussian distributed around a point?

The reason behind the spread of the point source object is due to the diffraction of the telescope's aperture. There is another diffraction effect from the atmospheric turbulence [14]-[17]. There is a particular limit after that the diffraction is dominated by atmospheric turbulence. The turbulence of the atmosphere is generated by the temperature gradient or pressure difference between two points. The effects of turbulence are in various ways. For example, the star which behaves as a point twinkle in the sky. That is because of the turbulence. This particular effects of turbulence on the point source are called as atmospheric seeing effect [14].

The atmospheric seeing effect shows the speckle like the structure of the point source with Gaussian distribution [16]. The more the turbulence, the more number of speckles inside the image. That will make the image blurry.

(1) Diffraction-limited to telescope aperture

The diffraction of the point source due to telescope aperture is given by, $\frac{1.22\lambda}{D}$. Where D is the diameter of the aperture in the meter. λ is the incident wavelength of the light in meter [15].

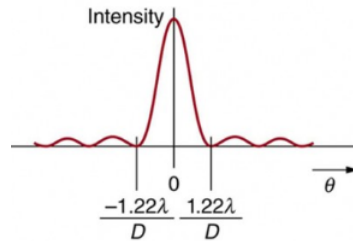


Figure 47: Distribution of the intensity due to diffraction-limited by telescope

From figure 47, it is apparent that diffraction plays a role in this distribution. This distribution almost follows the Gaussian distribution with different standard deviation and mean value. Most of the distribution (80 %) are fall in radius of $\frac{1.22 \cdot \lambda}{D}$. In this model, the intensity outside this radius is ignored [14]-[15]. The magnitude of this Gaussian distribution is obtained by the satellite's influx of the photons on the telescope. The standard deviation is defined by the fwhm (full width half maximum). fwhm is a width where intensity becomes half of its peak or maximum value. Generally, the fwhm of this diffraction effect is given by, $\frac{1.028 \cdot \lambda}{D}$. This fwhm varies with wavelength and diameter. From fwhm, the standard deviation of Gaussian profile is found by $\sigma = \frac{fwhm}{2.355}$. And the maximum radius of the point source image on CCD would be equivalent to $\frac{1.22 \cdot \lambda}{D}$ [54]-[55]. After deciding the magnitude, standard deviation, and maximum radius of the point source, it is put into the standard Gaussian equation. Here mean value is zero because the center is assumed as the origin point. The Gaussian equation is given by,

$$y = N \cdot e^{-\frac{x^2}{2 \cdot \sigma^2}} \quad (20)$$

Here, N is the magnitude of the intensity in the ADU unit. To describe or project the distribution in 1024 X 1024 pixels CCD, the σ , and fwhm should be calculated in terms of pixels. And there would be two variables x and y for the two dimensions (columns and rows).

Suppose, the satellite covers circular size with a diameter in 10 pixels. That means the radius of the point will be 5 pixels. In the diffraction $\frac{\lambda}{D}$ is a unit that remains constant for constant diameter and wavelength. If the wavelength is changed, the diffraction will be changed accordingly but the ratio between the radius of the point source and fwhm will be remained the same. Thus, using that concept, the satellite which covers a 5-pixel circular point source will have fwhm around $1.028 \cdot \frac{5}{1.22}$. Here 1.22 is equivalent to point with a radius of 5 pixels and 1.028 is fwhm of the diffraction-limited by the aperture. And that is equal to 4.21 pixels means the width of the Gaussian distribution where the intensity becomes half of its maximum value. Therefore, 4 pixel is the fwhm. The standard deviation of the distribution will be 1.78 or 2 pixels. The below figure shows the image of the point source satellite with covering 5-pixel radius circular disk in Gaussian distribution. Each pixel is illuminated by a given grayscale which follows the Gaussian profile.

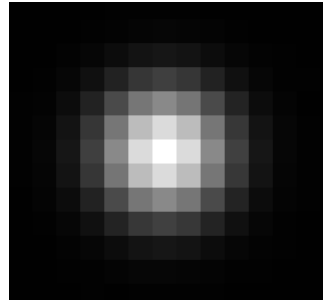


Figure 48: Distribution of the intensity due to diffraction-limited by a telescope on CCD

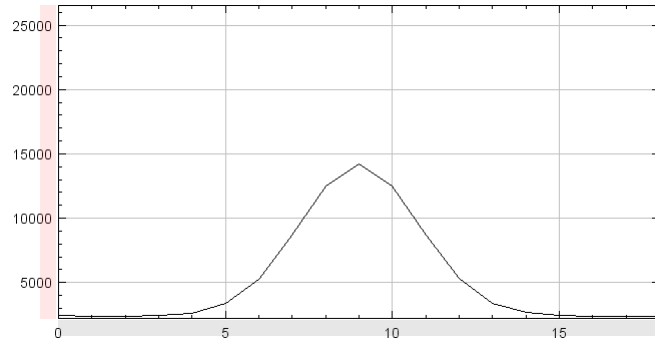


Figure 49: Gaussian distribution of the intensity due to diffraction-limited by telescope

In the above figure, the diameter of the distribution is almost 10 pixels. Also, the maximum value of ADU is 50000 on a grayscale. This effect of diffraction is related to telescope aperture. The ADU unit is explained in further sections.

(2) Atmosphere seeing effect and diffraction

As mentioned before, the atmospheric seeing effect is due to the turbulence. If the intensity of turbulence is not very strong then diffraction is limited by telescope aperture but if the intensity is strong then diffraction is limited by atmosphere seeing effect [14]. As the light wave propagates through the atmosphere it experiences fluctuations in amplitude and phase. An image

3 METHODS AND RESULTS

formed by focusing this wave exhibits fluctuations in intensity, sharpness, and position which are commonly referred to as scintillation, image's blurring, and image's motion. The diffraction angle is given as, $\theta = \frac{3.812 \cdot 10^5 \cdot \lambda}{r_0}$. The angle is given in arc second and r_0 is fried parameter which is the variable with turbulence intensity. The fwhm is given as $\text{fwhm} = \frac{2.013 \cdot 10^5 \cdot \lambda}{r_0}$ [14]-[17].

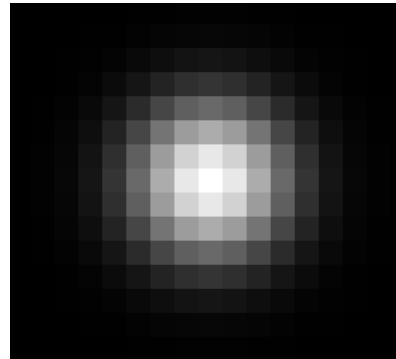


Figure 50: Gaussian distribution of the intensity due to diffraction-limited by atmospheric seeing effect

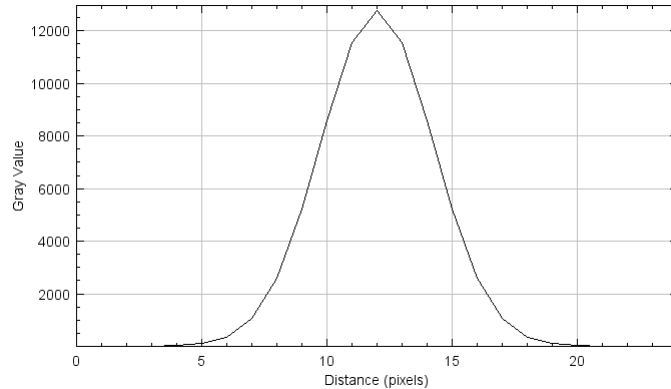


Figure 51: Gaussian distribution of the intensity due to diffraction-limited by atmospheric seeing effect

As mentioned earlier about the equivalent size of point' radius in terms of pixels in diffraction due to telescope aperture, the same concept is applied here. Suppose the circular point has 5 pixels radius size. Therefore using

$\text{fwhm} = 2.013 \cdot \frac{s}{1.906}$, the fwhm in terms of pixels would around 5.2 pixels or 5 pixels. Here 1.906 and 2.013 are the radius and fwhm of point in a unit of $\frac{\lambda}{D}$, respectively. The σ standard deviation would be $\sigma = \frac{\text{fwhm}}{2.355}$ and that would be 2.23 pixels. From the diffraction due to telescope aperture, the fwhm was 4 pixels and due to turbulence, the fwhm is 5 pixels. The profile of Gaussian distribution is described in the figures 50 and 51. It is apparent that the turbulence effect or diffraction due to turbulence makes the point source very blurry compared to aperture diffraction.

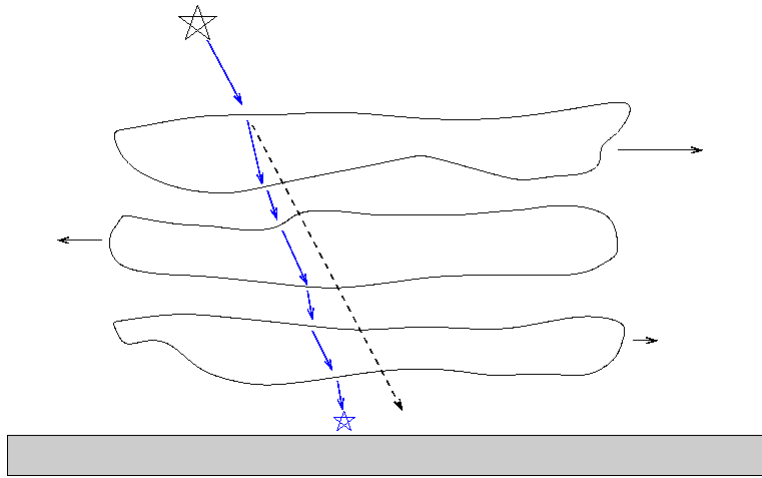


Figure 52: The blurring and scintillation of the star due to atmospheric seeing effect

In figure 52, the turbulence changes the wavefront of the incoming light and deviates the position of the star. Also, it makes the image blurry. But, turbulence is a very dynamic process, therefore, the movements of this star would be continuous. The blurriness and speckle formation of the point object will look like the below figure 53 ([16] and [17]),



Figure 53: The blurring and scintillation of the star due to atmospheric seeing effect

But these effects of speckle and motion are ignored in the model to avoid more complexity. So this effect is dominant when the turbulence is very strong. At last, the fried parameter is given by,

$$r_0 = [0.184\lambda^{\frac{6}{5}} \cdot (\cos\gamma)^{\frac{3}{5}} \cdot \int dh \cdot C_n^2(h)]^{-\frac{3}{5}} \quad (21)$$

The unit of the r_0 is in meters. λ is the wavelength in meters. γ is the zenith angle which is 90 - the altitude of the satellite. h is the altitude of the object in meters. $C_n^2(h)$ is the refractive index structure coefficient at a specific altitude.

$C_n^2(h)$ is given as, $C_n^2(h) = C_T^2 \cdot \left[7.9 \cdot 10^{-5} \cdot \frac{P}{T^2}\right]^2$ [14]-[17]. P is the atmospheric pressure in millibars and T is the temperature in K. Now C_T^2 is the temperature structure coefficient. And it is defined by, $C_T^2 = \frac{[T(x)-T(x+r)]^2}{r^{2/3}}$. Where x is a point within turbulence and r is another 3D distance from x . $T(x)$ is the temperature at given point [14]-[17]. It is evident that higher energy turbulence breaks isothermal cells into smaller units, reducing the average distance between points of the same temperature: as turbulence becomes more extreme, the average C_T^2 becomes smaller [16]-[17]. The fried parameter contains turbulence intensity, refractive index, pressure, wavelength. After all these parameters, the value of the fried parameter is calculated.

Based on the fried parameter, as mentioned, it could define the dominant diffraction effect. In the final image, the cumulative effects of both diffraction are present but one of the effect is dominant and it is determined by the condition. The conditions are given below,

$$(1) \frac{D}{r_0} > 1$$

3 METHODS AND RESULTS

If the condition (1) is satisfied, the diffraction is limited to the atmosphere seeing effect [14]. In condition (1) the D the diameter of the aperture is larger than the fried parameter. Therefore, turbulence will affect the point source diffraction. The fried parameter is equivalent to the object's wavefront which produces the diffraction. Similarly, the second condition is,

$$(2) \frac{D}{r_0} < 1$$

Here the diameter is less than the fried parameter. Thus telescope aperture affects the diffraction of the point source object [54] [55] and [15]. In the model, the $T(x+r) - T(x)$ is taken as 0.01 K with r is 1 m. The pressure P is taken as 300 millibars which is equivalent to 1 atm. The altitude is taken as 500000 meters, the average distance between LEO satellite and observer. λ is taken as 500 nm in the visible range. The average temperature is taken as $T = 250$ K. After considering all these values in the equation 21. The fried parameter r_0 comes out as 0.1189 m which is equal to 11.89 cm. That means turbulence brings the condition number (1) and diffraction will be dominated by atmosphere seeing effect. So this was the effect of diffraction on point source image in CCD image processing.

The size of the point image depends on the distance and real size of the satellite in the space. To find the radius of a point on CCD in terms of a pixel, the resolution of CCD is used to discern the smallest distance on it [56]. Suppose CCD has 1024 x 1024 pixels and the field of view of the site is around 0.05×0.05 degrees. Therefore, the resolution of a pixel would be $\frac{0.05}{1024}$. The unit of this resolution is a degree per pixel. That means each pixel covers around $5 \cdot 10^{-5}$ degree. Based on that, the radius of a point image is determined using this resolution. Now the real size of the satellite is come into the picture to calculate the point size on CCD in terms of pixels. Suppose the radius of the satellite is around 25 m. Also, the distance between observer and satellite should be taken to calculate the angular size of the 25 m size satellite. Here, the satellite is taken as a sphere or circular in shape. And the distance between observer and satellite is around 480 km. To calculate the angular size of the satellite radius in degree, the ratio between radius and distance is taken [56]. Therefore, the calculation will be $57.2958 \cdot \frac{25}{480000}$ and that is around 0.0029841 degree. Now using an angular resolution of CCD which is mentioned before around $5 \cdot 10^{-5}$, the radius of satellite in pixels is calculated. The angular size of satellite and resolution is divided and the answer is $\frac{0.0029841}{5 \cdot 10^{-5}}$ and that is around 60 pixels. That means 60 pixels are

equivalent to the radius of $\frac{1.22\cdot\lambda}{D}$ or 1.22 unit. The general formula is given by, $\frac{\theta\cdot P}{D}$. θ is the angular size of the satellite in degrees and D is the radius of the satellite in meters. Also, P is the total number of pixels. Sometimes the CCD is not in perfect square shape. It could be a rectangle shape with different pixels vertically and horizontally. Suppose the CCD has 1024 x 620 pixels. Based on that, the field of view will be changed but that will not differ the point size on CCD. The final part is image processing the trails using the model. The steps are explained in the below section.

3.2.6 Image processing

The image processing is the conversion of analog form voltage or a number of electrons to digital form [57]-[59]. The output of CCD is in voltage based on a number of electrons. Higher the electrons in each pixel are, the higher the voltage is. But CCD has a limit for each pixel around 10000 to 500000 electrons. Beyond that point, CCD will transfer electrons to the next pixel and create an effect called as blooming [10] and [60]. This blooming effect is undesirable and it could be avoided by setting the proper gain or exposure time.

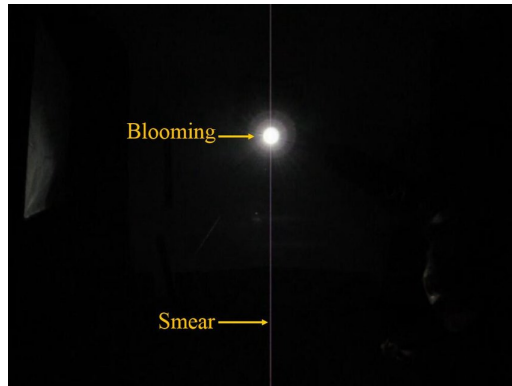


Figure 54: The blooming effect in CCD

In figure 54, the pixels are saturated with a total capacity. Beyond that capacity, it will pass the extra electrons to the next place and this chain process will continue until it gets saturated properly. But in this model, the exposure time and full well capacity is the most useful parameter to avoid this kind of phenomena.

3 METHODS AND RESULTS

CCD chip has a size of around 20 to 50 mm in width and length. The pixel has a square shape with a size of 20 to 40 microns. The resolution depends on the pixel's size. The small size pixels capture the influx of photons from the distant object. The very far star will have less flux of the photons, but increasing the exposure time could make the image more bright. But in our model, the output is the magnitude of the satellite. The magnitude is convertible into flux and from the flux, we can find the number of photons which are imparted on CCD chip's single-pixel.

The flux is found by below formula,

$$\frac{F_1}{F_2} = 10^{\frac{m_2 - m_1}{2.5}} \quad (22)$$

F_1, F_2 are fluxes for star 1 and 2. We know flux of sun $1376 \frac{W}{m^2 s}$ on average [20]. So, we could sun as a reference star and F_1 becomes 1376 and $m_1 = -26.58$ magnitude. But here in the model, the output of the magnitude is in the visible range. It is not possible to consider the whole range of wavelengths. Therefore, the flux density is very important. In astronomy, Jansky unit is useful to define the spectral flux density. ([20] and [61])

Also, the apparent magnitude of Vega star is around 0.0 and it is very easy and comfortable to use this value. Because the sun's magnitude and flux vary with earth's orbital and axial rotation. But the flux of the Vega remains constant because of its large distance. Thus, in the equation 22, the m_1 becomes 0.0 [62]. To calculate the average flux density in the visible range for the Vega star, it is very useful to consider the bandwidth of the visible range. The bandwidth of the visible spectrum is around 880 \AA^0 . And the central wavelength of the spectrum is 5440 \AA^0 . Based on these values, the flux from the Vega star in the visible range is found. The F_1 flux density is $363.1 \cdot 10^{-11} \frac{\text{erg}}{\text{cm}^2 \text{s} \text{\AA}^0}$ [63]. After multiplying this value with central wavelength and bandwidth, it will give the total flux in the visible range for Vega star. From the earlier equations, we can derive the magnitude of satellite m_2 . This will give the F_2 flux of that object. Reference star-like sun or vega has to be taken to calculate the flux of the satellite. After putting all values in equation 22,

$$F_2 = 363.1 \cdot 10^{-11} \cdot 10^{-\frac{m_2 + 0.0}{2.5}} \quad (23)$$

From flux, photon number is easily obtained using $E = h\nu$ (where $\nu = \frac{hc}{\lambda}$), area of telescope and exposure time. The unit of flux is per unit area unit

3 METHODS AND RESULTS

time and unit wavelength. But the flux is given in erg and that is converted into joule. Multiplication with central wavelength will make the unit of flux per unit time and area. The central wavelength is taken in the mid visible range. Time is the integration time or exposure time of the system. And the last one is the area of telescope aperture. The incoming photons which are coming from the star or satellite always come through the telescope aperture. After the optics manipulation, the flux is concentrated on some parts of pixels on CCD. The multiplication of these parameters will give the final total number of photons.

Wavelength is the incident photon color's property. Here, magnitude is in visual band, therefore, the bandwidth of the visible range is multiplied. The final equation is given by,

$$n = \frac{F_1 \cdot \lambda_{central} \cdot \lambda_{bandwidth} \cdot 10^{-\frac{m_2+0}{2.5}} \cdot TA}{hc} \quad (24)$$

From the equation, $\lambda_{central}$ is the central wavelength of the visible band around 5440 Angstrom. $\lambda_{bandwidth}$ is the bandwidth of the visible range around 880 Angstrom. After putting the values inside the equation 24,

$$n = \frac{363.1 \cdot 10^{-11} \cdot 5440 \cdot 880 \cdot 10^{-10} \cdot 10^{-\frac{m_2+0}{2.5}} \cdot TA \cdot 10^{-7}}{hc} \quad (25)$$

In the equation, 10^{-7} is the conversion factor from erg to joule unit. The factor 10^{-10} is the conversion scale from Angstrom to meter. After putting exposure time around 1 s, area of the telescope aperture in cm^2 as $\pi \cdot 0.6 \cdot 0.6 \cdot 10000$ (where 0.6 m is radius of aperture), the satellite with apparent magnitude around -3.0 will have the total number of photons 156847111149.45316 and that is the very big number. Here the radius of the aperture is taken as 0.6 m. This large number is the total number of photons coming from the star or satellite with -3 apparent magnitude in visible range towards the 0.6 radii aperture within 1 s of exposure time. That's the shortest explanation of the total number photons to the CCD.

From the equation 25, it is apparent that exposure time is again playing very important role to change the flux accordingly. In astronomy, the exposure time varies from object to object. It could have ms or hours as a unit. But the CCD doesn't count the exact number of photons. On CCD,

3 METHODS AND RESULTS

each pixel will be illuminated with photons and these photons are converted into electrons to measure the brightness of the star in form of the voltage. But during the conversion of photon to electron by silicon diode in a pixel, some of the photons are converted into electrons. That means, if the pixel is getting around 1000 photons that doesn't mean the converted electrons will be the exact 1000. It could be 500 or 700 based on the efficiency of the CCD. That efficiency is called the quantum efficiency [64] and [10]. The quantum efficiency just gives the wrong number of flux, not the wavelength (It only affects the illumination of the object). Thus, quantum efficiency is multiplied with total number of photons to find the generated electrons in a pixel. The equation will become $n_e = Q.E. \cdot n$, where n is the incident photon number and Q.E. is the quantum efficiency. The final converted electrons will be n_e . This quantum efficiency is dependent on the wavelength which is incident on the CCD. Here it is given the variation of the quantum efficiency with wavelength [64],

From the table 6, it is apparent that in the visible range or visible wavelength line 550 nm, the quantum efficiency is around 60 %. That means in the incident of 100 photons with a wavelength of 550 nm, the 60 electrons will be generated. The actual value of the pixel changes due to quantum efficiency.



Figure 55: Quantum efficiency in CCD

Table 6: Quantum efficiency variation with wavelength

Wavelength (nm)	Quantum efficiency
-----------------	--------------------

Wavelength (nm)	Quantum efficiency
307	5.96
323	8.93
336	11.91
349	15.88
360	19.85
370	23.33
380	27.3
399	30.277
425	32.74
443	35.72
454	40.18
464	44.65
475	47.13
485	45.63
498	43.64
514	46.61
524	49.59
537	53.56
553	59.02
566	62.49
574	66.47
582	66.96
589	66.96
608	62.96
634	64.43
665	63.42
683	58.93
697	53.94
717	50.94
741	50.43
757	45.94
767	41.95
783	37.46
796	32.98

Table 7: Quantum efficiency variation with wavelength

Wavelength (nm)	Quantum efficiency
817	32.46
843	31.45
874	27.94
895	25.44
913	20.95
924	17.46
937	14.47
950	9.98
971	6.48
997	7.46

Figure 55 is showing the trend of quantum efficiency with wavelength. The trend is very unusual but it follows almost quadratic nature. The maximum efficiency (68 %) is at 580 nm.

After considering, the white noise, readout noise, flicker noise, dark noise, shot noise, sky background and its related noise, quantum efficiency, exposure time, bandwidth, visible wavelength, the final number of photons are obtained using the final equation 25 with the multiplication of quantum efficiency. In the CCD, the electrons or voltage is an analog form which is needed to be converted into the digital form. In the conversion process, the transformation from analog to digital occurs with a particular frequency. If the frequency of this conversion is not at a certain limit, it will make the image blurry and very unclear. This effect is called the Aliasing effect [19]. Aliasing is the process or effect that occurs in every signal processing like here in the CCD.

The voltage form of the CCD is the sample and this sample should be uniquely converted into digital or indistinguishable parts such that it looks like a continuous form like the original sample in analog form. The aliasing effect has two types: the temporal and spatial effects. In the satellite trails simulation, the spatial aliasing effect will occur.



Figure 56: The Aliasing effect during the sampling process

In the above figure, it is a spatial aliasing effect where the original analog form is not properly sampled during the processing inside the camera. The edges of the cherry are very clear from the figure. To reduce it, there are filters for the anti-aliasing effect to reduce it.

The aliasing effect occurs when the sampling rate is below a certain limit. This is called Nyquist frequency which states the theorem [18]. It is very useful for the digitization of the continuous form image. This frequency which is frequently mentioned here called sampling rate or a number of samples per second. The theorem says the sampling rate should be equal or higher than the $d/2$. Where d is the smallest object or resolution. The Nyquist theorem states that in order to adequately reproduce a signal, it should be periodically sampled at a rate that is 2X the highest frequency you wish to record [18]. With images, frequency is related to structure size. Small structures are said to have a high frequency. If the frequency is less than this limit, the aliasing effect will dominate the image.

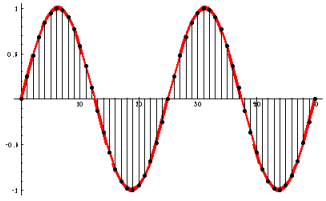


Figure 57: The sampling frequency greater than the limit or oversampling

This is oversampling and it will not make the image bad but the data samples will become such large that it would take time to get output.

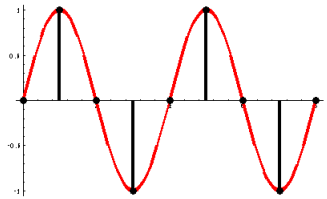


Figure 58: The sampling frequency equal to the limit

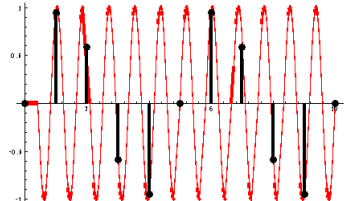


Figure 59: The sampling frequency less than to the limit or under-sampled

In the under-sampled rate, the aliasing phenomena shows its nature into the image [65]. In the model, the aliasing effect is removed by considering the image or satellite as point source function with Gaussian distribution.

Now the last step remains to convert the number of electrons into the ADU or digital unit form using the pixel's well capacity. Normally, the pixel's well capacity is around 100000 to 1000000 electrons. Beyond this capacity, it will show the blooming effect which is mentioned above in figure 54. And that

problem is solved by adjusting the exposure time or gain the capacity of the well.

In astronomy, the output of the image is in the grayscale. In short, it looks like a black and white image. The astronomer converts this grayscale image into the color image by passing or converting them using color band-pass. They use green, red, and blue pass filters to create the color image. The grayscale image comes in 16 bit int or float type or 8-bit int or float. The higher the bit size, the higher the resolution of the image. Thus, the 16-bit image has a high resolution than an 8-bit image. In the 16 bit or 8 bit image, the possible gray value of each pixel will be $2^{16} - 1$ or $2^8 - 1$ which are equivalent to 65536 or 255 [57]-[59]. Therefore, the 65536 is the maximum gray value in the 16 bit CCD and it will denote the color almost white. The collected electrons is converted into the gray value by simple ratio, $ADU = 65536 \cdot \frac{n_e}{100000}$. The answer is in ADU (Analog to Digital Unit). Here 100000 is the maximum well capacity which could be held by a pixel. 65536 is the maximum gray value of the 16 bit CCD, and n_e is the collected electrons from the point or extended source from the sky. Suppose, the $n_e = 10000$ then the gray value for that pixel would be 6553, not 6553.6 because it is 16-bit int, not 16-bit float. Therefore, the associated gray value will be given to that pixel [57]. After considering, apparent magnitude, atmospheric extinction, aliasing effect, point source function, different noise, and quantum efficiency, the satellite trails are formed using Python. Before simulating the satellite trails, the field of view is an essential factor to take picture of satellite trails.

3.2.6.1 Field of view The trails are generally viewed in the range of 0.1 to 0.05 degrees. But to calculate the field of view for the different telescopes is a crucial thing. Because different telescope has the different magnification and this magnification decides the field of view [26] and [69]. The field of view is calculated by several parameters. The first one is $f\#$ number and it is the ratio of the system's focal length to the diameter of the entrance pupil. $f\#$ is defined by $f\# = f \cdot M$. Where M is a magnification of the telescope and f is a constant number when the magnification of a telescope is one. The telescope observatory at PRL has $f = 13$. And $f\#$ would vary with magnification M . The diameter of the telescope is D and it is around

1.2 meters or 1200 mm. The CCD chip inside the telescope has 1024 pixels and the size of a pixel is 13 micron. Using $f\#$ and D , the plate scale of the telescope is found. The plate scale of a telescope connects the angular separation of an object with the linear separation of its image at the focal plane. That means it gives the relation between angular size with linear scale size. The plate scale is given by, $\text{plate scale} = \frac{206265}{D f\#}$. The unit of the plate scale is arcsec/mm. Because D is mm and 206265 value is in arcsec. If the D is 1200 mm and $f\#$ is 13 with magnification $M = 1$ then plate scale will be 13.222 arcsec/mm. That means, 1 mm is equivalent to 13.22 arcsec [26] and [69].

Now, to find the angular size per pixel, the multiplication of the size of the pixel would be taken to get it. Therefore, per pixel, the scale would be $\text{plate scale} \cdot \text{size of pixel}$. Suppose, the size of the pixel is 13 micron or 0.013 mm. Putting the value in the plate scale equation, we would get 0.172 arcsec per pixel. That means one pixel covers 0.172 arcsec. To find the field of view of the CCD chip, we have a total of 1024 pixels. Thus, the field of view of telescope or CCD chip would be multiplication of a total number of pixels and plate scale per pixel. The equation would become $\text{fov} = N \cdot \text{plate scale}$. Here N is a total number of pixels and fov is the field of view. From the standard values as mentioned earlier, the field of view with given values will be 176.012 arcsec or 0.0489 degrees [26] and [69].

From the intuition, it is clear that magnification changes the field of view in bigger and smaller size. The higher the magnification is, the lower the field of view. Suppose in the above problem, the magnification is 0.48 with the same parameters of pixel's size, the total number of pixels and diameter of the telescope, the field of view would become 0.1 degrees. Using this concept, the field of view is set to 0.05 degrees in the result of satellite trails. The results of the satellite trails for different satellites are given in the next subsection.

3.2.7 Result of satellite trails

(1) ISS (Zarya) Satellite trails: The trails of the satellite are obtained by considering the aforementioned factors. The specification of the image of trails is given as follows: The field of view is taken as 56.68 X 56.72 in degrees for altitude and 285.72 X 285.77 degrees in azimuth. That means the sky is covered in a range of 0.05 X 0.05 degrees assuming that CCD chip is a square. Also, the diameter of the telescope aperture, pixel's size,

3 METHODS AND RESULTS

and a number of pixels are taken as 1.2 m, 13 microns, and 1024 X 1024. The satellite trails are simulated during 2020/6/5 at 6:53:34. The average distance between observer and satellite is around 508 km and the time of flight of the satellite within the field of view is around 0.04 seconds. The CCD is assumed to be 16 bit with a well capacity of 100000 electrons.

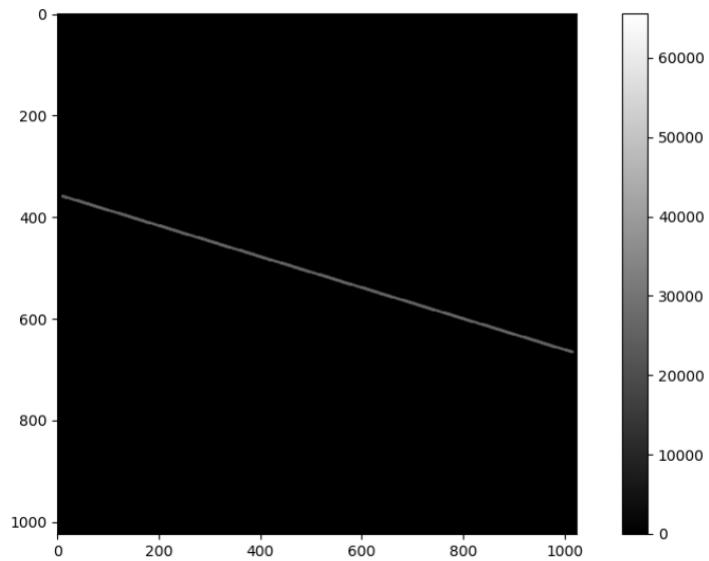


Figure 60: The image of trails during the flight of the satellite ISS

From figure 60, it looks like the satellite is not clearly visible even if the distance is around 507 km. The reason is the phase angle of the satellite with sun and observer. The less phase angle couldn't illuminate the satellite properly. But the maximum digital form or ADU of each pixel is around 26000. Also, the satellite passed through this view within 0.04 seconds.

3 METHODS AND RESULTS

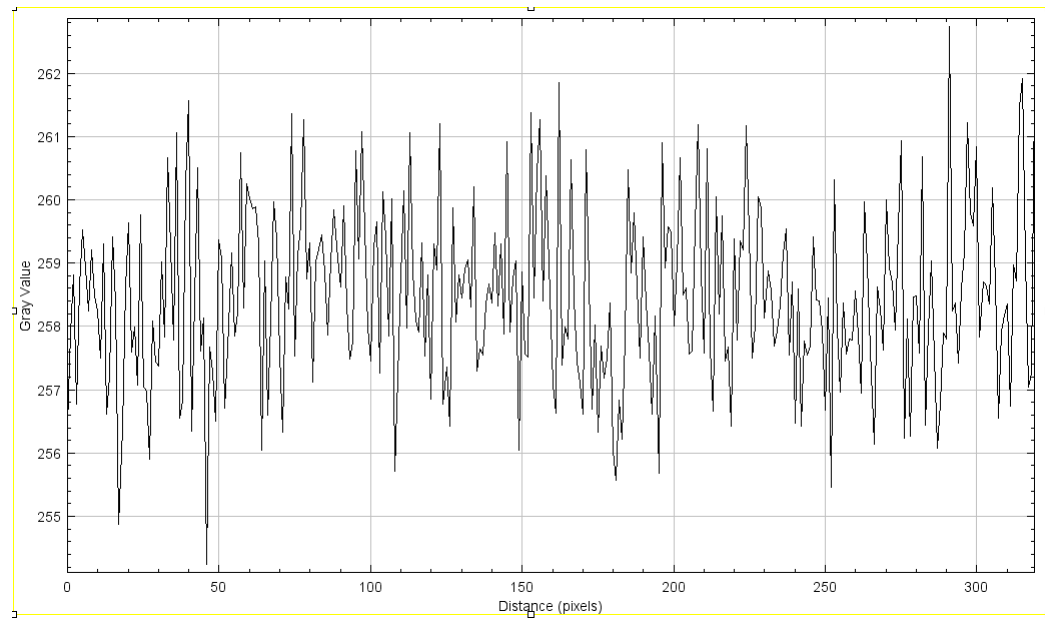


Figure 61: Noise distribution

In figure 61, the y-axis describes the ADU value of the frame. The noise is very random due to the distributions. This profile includes all the above-mentioned noises.

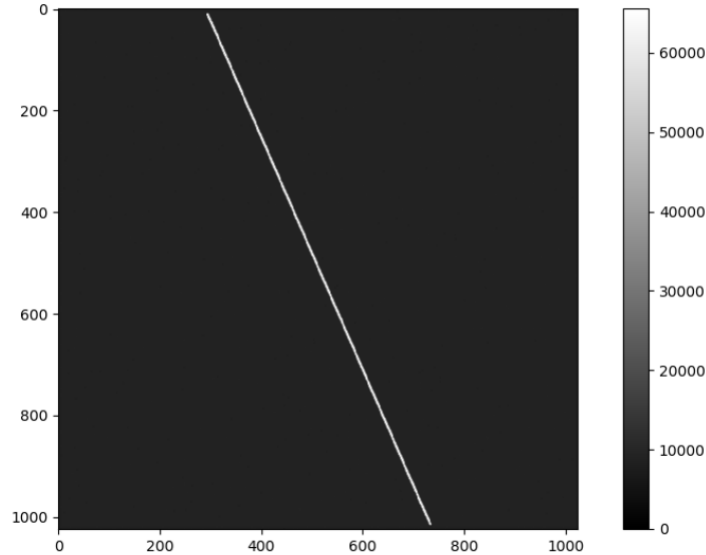


Figure 62: Satellite trails of ISS

The above figure shows another trail of the same satellite. This time the illumination is higher than the first image. The satellite trails model is designed in such a way that the satellite would pass through the center of the field of view.

Now the satellite trails of the debris would be invisible with the naked eye because of the high apparent magnitude. The average size of the debris of Iridium 33 is around 10 to 50 cm [38]. And the albedo of this debris is around 0.2 to 0.5 depends on the surface. The satellite trails of the debris are obtained on 2020-7-2 at 22:50:34 UTC. The field of view is the same at 0.05 degrees. The altitude and azimuth are in the range of -43.2 to -43.15 degrees and 183.96 to 184.01 degrees, respectively. The average distance between observer at 23.0143, 72.7751, and debris is 780 km. And the passing time of the debris within the field of view is around 1.54 sec. Here the size is taken around 2 m to make it visible in the result.

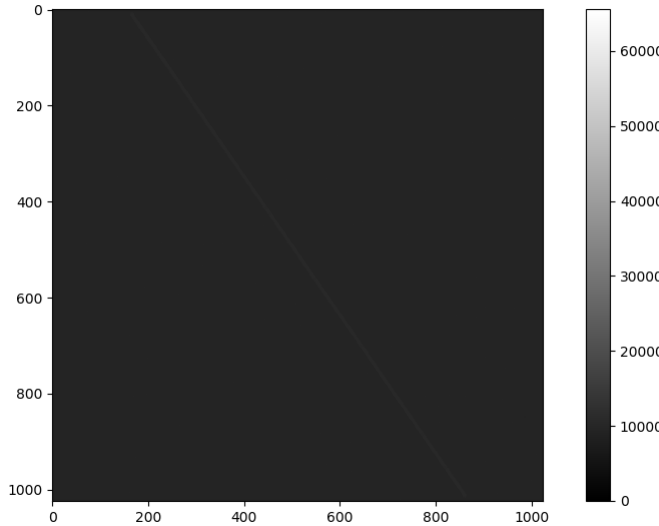


Figure 63: Satellite trails of Iridium 33

The satellite trails of the debris are at a maximum of around 15000-20000 ADU. Also, the geosynchronous satellite is very hard to see with the naked eye. Therefore, the results of the trails are promising to describe its motion and TLE which is described in the next section.

3.2.8 Simulation of the trajectory of the satellite

The simulation of the trajectory of a particular satellite is done in this sub-part. The simulation is a kind of animation of the vector position of a satellite with time. The data input is the coordinates in the ECI reference frame. As mentioned earlier, the ECI frame gives the output in XYZ coordinate with certain reference points. The reference axis, the vernal equinox, is also represented in the vector form. Also, the position vector of the observer's location is described in the animation. The animation is done for two satellites: ISS (Zarya), Iridium in Python. The result of the animation for ISS (Zarya) satellite is shown below, The simulation of a trajectory vector is obtained from 2020-7-2. The satellite completes a full round around the earth within 90 minutes on the given day. The simulation is given in the below link,

<https://gitlab.com/rid181198/space-debris-simulation/-/blob/75babf5d3de71818d65a47c521632277a3464f1d/Simulation%20of%20trajectory/ISS.gif>

In the animation, the yellow color vector position represents the ISS (Zarya) satellite. The blue color vector position represents the observer. And the green one is vernal equinox direction. The rotation axis of the given sphere or earth is perpendicular to the vernal equinox direction in upward. From the animation, the speed of the satellite is very faster than the observer. Also, the observer's speed is the rotation speed of the earth. The speed of the satellite is around 7.65 km per second.

The other satellite debris (Iridium) simulation is given in the below link,

<https://gitlab.com/rid181198/space-debris-simulation/-/blob/75babf5d3de71818d65a47c521632277a3464f1d/Simulation%20of%20trajectory/IRIDIUM.gif>

In the animation, the red color vector position represents the Iridium satellite. Also, the simulation or animation is obtained from 2020-7-2. If the simulation of trajectory for both satellites is considered in the single frame, the simulation would look like in below link,

https://gitlab.com/rid181198/space-debris-simulation/-/blob/75babf5d3de71818d65a47c521632277a3464f1d/Simulation%20of%20trajectory/ISS_PLUS_IRIDIUM.gif

In the simulation, the trajectories of both satellite and debris are shown on 2020-7-2. This simulation is only for the understanding of the satellite's trajectory and visualization.

4 Future scope: TLE from optical observation of the satellite

TLE of any satellite body comes from the optical observations of the trails in the sky. Using various algorithms and observations, TLE of the satellite

orbit is determined. The most major orbital elements are inclination, ascending nodes, eccentricity, mean anomaly, semi-major axis, mean motion, and argument of perigee. To get these elements, fundamental variables like velocity, position, distance from earth's center are necessary to know for the algorithm. The multiple observation could determine the drag and other perturbations of the trajectory. Many software and algorithms are made to get TLE of the satellite [66], [67], [68]. People have worked upon this field but the perturbations and B star coefficient are hard to get. Using the results of SGP4 model and simulation of trails, this kind of algorithm is helpful to get precise TLE by providing constraints. So this work would be appreciable in future studies.

5 Discussion and Conclusion

Using the SGP4 model, the satellite's position is easily found using mathematical equations and some perturbations. The accurate results of the model describe the inclusiveness and flexibility. The results in Alt-Az and Ra-Dec for ISS (Zarya), Iridium, and QZS - 1 satellite are found with the help of the model. The generated results are further used in the simulation of the satellite trails. The simulation of trails is obtained through considering the CCD's noises, atmospheric extinction, diffraction due to turbulence and telescope aperture, apparent magnitude, quantum efficiency and albedo of the satellite.

The noises of CCD contain readout, dark, shot, sky background noise. Also, the satellite is assumed to be a circular point source in the sky. And the point source function which follows the Gaussian profile has been taken for the imaging. The point source is diffracted by turbulence and telescope aperture and its effect on fwhm is also taken. Then the illumination of the pixels on CCD is considered and its relation with incident photons. The ADU unit and gray value are associated with incident photons or apparent magnitude of the source. The ADU is the digital output of the CCD. Also, the apparent magnitude is attenuated by the atmosphere due to scattering and absorption of the light. The atmospheric extinction, noise, diffraction, and digital form of the CCD's pixels voltage form generate the satellite trails within a certain field of view which depends on the magnification of the telescope.

After the satellite trails, the inclination, eccentricity, ascending nodes, mean

motion, and other satellite orbital elements could be found using the observational study of the satellite. These observations provide information about the TLE of the satellite. The future work on the generation of TLE from the observational data of satellite trails is excellent. Also, the problem of a collision between satellites and the generation of debris could be solved if the futuristic trajectory of the satellite is known. Also, there are other models for geosynchronous satellites and incoming satellite in the earth's atmosphere. Using these models, the future of the satellite object is determined and these are the future works in this field.

References

- [1] Aditya Chaturvedi. *Do you know how many satellites are currently orbiting around the Earth?*, <https://www.geospatialworld.net/blogs/do-you-know-how-many-satellites-earth/#:~:text=In%20the%20history%20of%20satellites,around%20planets%20other%20than%20earth.,> 2019.
- [2] Jonathan O'Callaghan. *What is space junk and why is it a problem?*, <https://www.nhm.ac.uk/discover/what-is-space-junk-and-why-is-it-a-problem.html>, 2019.
- [3] Donald J. Kessler Burton G. Cour-Palais. *Collision frequency of artificial satellites: The creation of a debris belt*, <https://doi.org/10.1029/JA083iA06p02637>, Journal of geophysical research space physics, Vol. 83, pp. 2637-2646, 1978.
- [4] Max H Lane, K H Cranford. *An improved analytical drag theory for the artificial satellite problem*, American Institute of Aeronautics and Astronautics, American Astronautical Society, No. 69-925, 1969
- [5] David A. Vallado, Paul Cranford, Richard Hujasak, T. S. Kelso. *Revisiting Spacetrack Report 3: Rev 2*, AIAA 2006-6753-Rev2.
- [6] L. David and S.S.I. Columnist. *Space junk: Dealing with the orbital debris threat*, Available at: <http://www.space.com/19445-space-junk-threat-orbitaldebris-cleanup.html>, 2009.

REFERENCES

- [7] Felix R. Hoots and Ronald L. Roehrich. *Models for Propagation of NORAD Element Sets*, SPACETRACK REPORT NO. 3, 1980.
- [8] Peter Duffett-Smith. *Practical Astronomy with your calculator*, Cambridge University Press, ISBN 0 521 28411 2.
- [9] James R. Janesick. *Scientific charge-coupled devices*, SPIE Press. p. 4. ISBN 978-0-8194-3698-6, 2001.
- [10] Thomas J. Fellers and Michael W. Davidson. *CCD Noise Sources and Signal-to-Noise Ratio*, National High Magnetic Field Laboratory, <https://hamamatsu.magnet.fsu.edu>
- [11] Bell Labs. *Charge Coupled Device*, <https://www.bell-labs.com/about/history-bell-labs/>
- [12] Thomas Young. *The Bakerian Lecture: Experiments and calculations relative to physical optics*, <https://doi.org/10.1098/rstl.1804.0001>, 1804.
- [13] Kiarash Ahi. *Mathematical Modeling of THz Point Spread Function and Simulation of THz Imaging Systems*, IEEE Transactions on Terahertz Science and Technology, 747-754, 2017.
- [14] Lorenzo Zago. *Atmospheric seeing effect*, <http://www.eso.org/gen-fac/pubs/astclim/papers/lz-thesis/node11.html>
- [15] *Diffraction on circular apertures*, https://sites.ualberta.ca/~pogosyan/teaching/PHYS_130/FALL_2010/lectures/lect37/lecture37.html
- [16] Gaston Baudat. *Astronomical Seeing*, Innovations Foresight, LLC, 2016.
- [17] C.E. Coulman. *Astronomical Seeing*, Annual Reviews of Astronomy Astrophysics.
- [18] John W. Leis. *Digital Signal Processing Using MATLAB for Students and Researchers*, p. 82. ISBN 9781118033807, 2011.

REFERENCES

- [19] Fredric J. Harris. *Multirate Signal Processing for Communication Systems*, Upper Saddle River, NJ: Prentice Hall PTR. ISBN 978-0-13-146511-4, 2016.
- [20] Terry Herter. *Luminosity, Flux and Magnitudes*, [http://hosting.astro.cornell.edu/academics/courses/a290/lectures/A2290_13%20\(Flux%20and%20Magnitudes\).pdf](http://hosting.astro.cornell.edu/academics/courses/a290/lectures/A2290_13%20(Flux%20and%20Magnitudes).pdf)
- [21] Haingja Seo, Ho Jin, Yongjun Song, Yongseok Lee, Youngseok Oh. *The Photometric Brightness Variation of Geostationary Orbit Satellite*, J. Astron. Space Sci. 30(3), 179-185 (2013)
- [22] Chris McFee. *An introduction to CCD operation*, https://www.mssl.ucl.ac.uk/www_detector/ccdgroup/optheory/ccdoperation.html
- [23] Michael Richmond. *Atmospheric effects: extinction and seeing*, <http://spiff.rit.edu/classes/phys445/lectures/atmos/atmos.html>
- [24] M. JURADO VARGAS, P. MERCHÁN BENÍTEZ et al. *MEASUREMENTS OF ATMOSPHERIC EXTINCTION AT A GROUND LEVEL OBSERVATORY*, Astrophysics and Space Science, DOI: 10.1023/A:1015184127925, 2001.
- [25] C. Buton et al. *Atmospheric extinction properties above Mauna Kea from the Nearby Supernova Factory spectro-photometric data set*, Astronomy Astrophysics, 2012.
- [26] Edmund Optics. *Understanding Focal Length and Field of View*, <https://www.edmundoptics.com/knowledge-center/application-notes/imaging/understanding-focal-length-and-field-of-view>
- [27] Cool cosmos. *Coordinate Systems*, http://coolcosmos.ipac.caltech.edu/cosmic_classroom/cosmic_reference/coordsys.html
- [28] University of arizona. *Astrometry*, http://ircamera.as.arizona.edu/Astr_518/atomy.pdf
- [29] NASA. *Catalog of Earth Satellite Orbits*, <https://earthobservatory.nasa.gov/features/OrbitsCatalog#:~:text=There%20are%20essentially%20three%20types,farthest%20away%20from%20the%20surface.>

REFERENCES

- [30] Space Foundation. *Types of Orbits*, https://www.spacefoundation.org/space_brief/types-of-orbits/
- [31] T.S. Kelso. *NORAD Two-Line Element Sets Current Data*, CelesTrak.
- [32] David A. Vallado, Paul Crawford, Richard Hujasak, and T. S. Kelso. *Revisiting spacetrack report no. 3: Revision 2*, Astrodynamics Specialist Conference, 2006.
- [33] FELIX R. HOOTS, RONALD L. ROEHRICH. *Project space track*, Aerospace defense command united states air force, 1980.
- [34] Sumus Tracker. *Two-line element (TLE) format*, <http://www.stltracker.com/resources/tle>
- [35] Brandon Rhodes. *sgp4 2.12*, <https://pypi.org/project/sgp4/>
- [36] Ashby, Neil. *The Sagnac effect in the Global Positioning System*, Springer. p. 11. ISBN 1-4020-1805-3 ,2004.
- [37] Cabinet Office, Government Of Japan. *Quasi-Zenith Satellite Orbit (QZO)*, <https://qzss.go.jp/en/technical/technology/orbit.html>, 2018.
- [38] Iannotta, Becky. *U.S. Satellite Destroyed in Space Collision*. , Space.com, 2009.
- [39] Spectral Instruments. *What Is A CCD*, http://www.specinst.com/About_Us.html
- [40] Eastman Kodak Company. *CCD Image Sensor Noise Sources*, https://www.uni-muenster.de/imperia/md/content/ziv/multimedia/downloads/kodak__noise_sources.pdf, 2001.
- [41] Oxford instruments Andor. *iKon-M 934 CCD*, <https://andor.oxinst.com/products/ikon-xl-and-ikon-large-ccd-series/ikon-m-934#product-information-tabs>
- [42] Ilias Ntagioglou. *Optimizing exposure time in deep-sky imaging*, https://www.cedic.at/arc/c15/dwn/CEDIC15_L05_Ilias_Ntagioglou.pdf, 2015.

- [43] MicroscopyU. *CCD Signal-To-Noise Ratio*, <https://www.microscopyu.com/tutorials/ccd-signal-to-noise-ratio>
- [44] Mike Luciuk, Asterism.org. *How Bright is the Moon*, <https://asterism.org/2019/04/12/how-bright-is-the-moon/#:~:text=Our%20Moon's%20average%20visual%20albedo,an%20increase%20of%202.7%20magnitudes.>
- [45] The Sky Live. *The Moon*, <https://theskylive.com/moon-info>
- [46] Nick Strobel. *Magnitude System*, <http://www.astronomynotes.com/starprop/s4.htm>, 2010.
- [47] *Apparent and Absolute Magnitudes*, <https://www.phys.ksu.edu/personal/wysin/astro/magnitudes.html>, 1998.
- [48] Gary A. McCue, James G. Williams Joan M. Morford. *Optical characteristics of artificial satellites*, Planet. Space Sci., Vol. 19, pp. 851-868, 1971.
- [49] The university of melbourne. *Lunar phases and tides*, <https://indigenousknowledge.research.unimelb.edu.au/resources/mathematics,-moon-phases,-and-tides>
- [50] NASA. *International Space Station Zarya*, https://www.nasa.gov/mission_pages/station/structure/elements/fgb.html, 2014.
- [51] Observational Techniques for Astronomers. *Photometric Systems*, <http://slittlefair.staff.shef.ac.uk/teaching/phy217/lectures/principles/L04/index.html>
- [52] V. Mohan, W. Uddin, S. K. Gupta. *Atmospheric extinction at Devasthal, Naini Tal*, Bulletin of the Astronomical Society of India 27:601, 1999.
- [53] *POINT SPREAD FUNCTION (PSF)*, www.telescope-optics.net, Retrieved 2017-12-30.
- [54] University of Heidleberg. *Diffraction*, http://www.ita.uni-heidelberg.de/~dullemond/lectures/obsastro_2011/chap_diffract.pdf

- [55] Wikipedia.org *Full width at half maximum*, https://en.wikipedia.org/wiki/Full_width_at_half_maximum
- [56] W. Romanishin. *An Introduction to Astronomical Photometry Using CCD*, <http://observatory.ou.edu>, 2006.
- [57] Learning about Electronics. *Analog-to-digital Converter (ADC) Calculator*, <http://www.learningaboutelectronics.com/Articles/Analog-to-digital-conversion-ADC-calculator.php#answer>, 2018.
- [58] StackExchange. *What are ADU (analog-to-digital units)?*, <https://physics.stackexchange.com/users/11835/placeholder>
- [59] ELPROCUS. *How to Convert the Analog Signal to Digital Signal by ADC Converter*, <https://www.elprocus.com/analog-to-digital-adc-converter/>
- [60] Basic principles of image sensors. *Blooming*, http://www.optique-ingenieur.org/en/courses/OPI_ang_M05_C06/co/Contenu_14.html
- [61] Durham University. *Basic Photometry*, https://community.dur.ac.uk/physics.astrolab/photometry_theory.html
- [62] AstroPixels.com. *Vega*, <http://astropixels.com/stars/Vega-01.html>
- [63] Caltech. *MAGNITUDE AND COLOR SYSTEMS*, http://web.ipac.caltech.edu/staff/fmasci/home/astro_refs/magsystems.pdf
- [64] Andor, Oxford instruments. *How to Define the Quantum Efficiency of CCD Cameras*, [https://andor.oxinst.com/learning/view/article/ccd-spectral-response-\(qe\)](https://andor.oxinst.com/learning/view/article/ccd-spectral-response-(qe))
- [65] Starizona. *Harold Nyquist*, <https://starizona.com/tutorial/harold-nyquist/>
- [66] StackExchange. *How to programmatically calculate orbital elements using position/velocity vectors?*, <https://space.stackexchange.com/a/1919>

REFERENCES

- [67] Tiar Dani, Abdul Rachman. *Generating two-line elements (TLE) of artificial space objects from optical observations: Preliminary results*, DOI: 10.1063/1.4930674, Volume: 1677, 2015.
- [68] David Vallado, Vladimir Agapov. *Orbit Determination Results From Optical Measurements*, DOI: 10.2514/6.2010-7525, 2010.
- [69] Dale E. Gary. *Telescopes and Detectors*, <https://web.njit.edu/~gary/320/Lecture3.html>